# Quasi-Decadal Variations in the North Atlantic

by Ken-ichi Mizoguchi

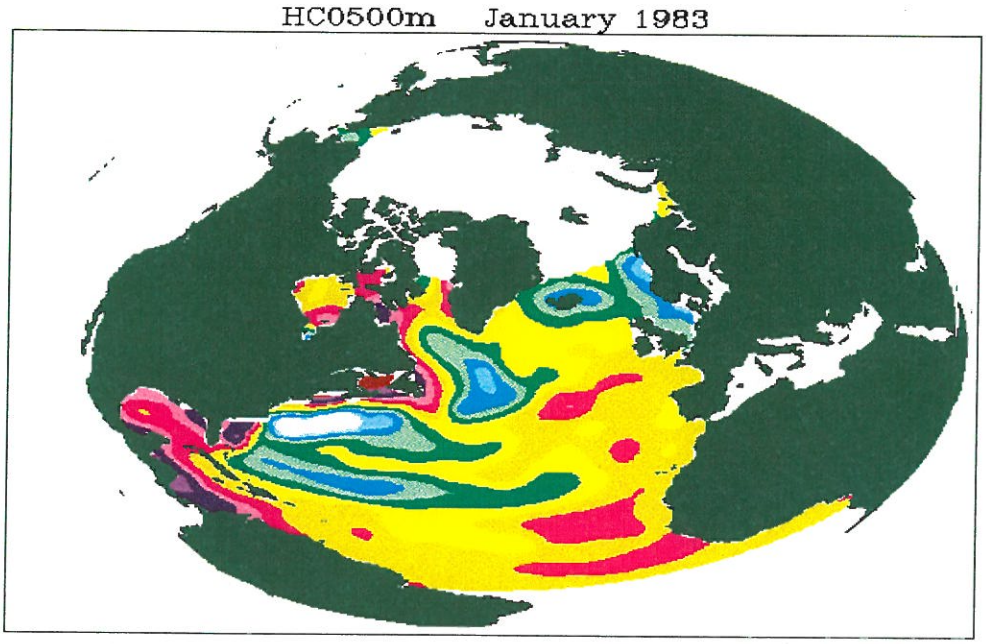


*Warm and Cold Anomalies in Upper 500m Heat Content*

The Center for Ocean-Atmospheric Prediction Studies
The Florida State University
Tallahassee, FL 32306-2840 USA

Dr. James J. O'Brien, Director

Technical Report 02-1

CENTER FOR OCEAN-ATMOSPHERIC PREDICTION STUDIES
THE FLORIDA STATE UNIVERSITY
TALLAHASSEE, FL 32306, USA
DIRECTOR: DR. JAMES J. O'BRIEN

# QUASI-DECADAL VARIATIONS IN THE NORTH ATLANTIC

By

KEN-ICHI MIZOGUCHI

DECEMBER, 2001
TECHNICAL REPORT

# TABLE OF CONTENTS

## FOREWORD

This is the Ph.D. of Dr. Kenichi Mizoguchi. It is a serious contribution to the understanding of the oceanic physics of the 10-14 years North Atlantic Oscillation. The model is an adequate modern model of the ocean/ ice system driven by 43 years of estimated atmospheric fluxes. The research explains the observed oscillation dynamical physics as it occurs in this model. Unfortunately the model resolution is only modest. The research will have to be redone with a high-resolution model in the future. However, despite this reservation, the results are quite exciting.

Dr. Mizoguchi used the technique called complex (or propagating) E.O.F. analysis to extract the information on the physical mode that characterizes the oscillation. It is a chicken &egg argument. Basically, internal Kelvin waves progress from the Labrador Sea to the equator of Brazil, across to Africa and north to the West Coast of Europe. Then Rossby waves radiate across to the East Coast of New England and Canada to recondition the Labrador Sea for the second half of the oscillation. Note: You need to read this report to understand the sign and thermodynamic processes that modulate the magnitude of deep-water formation in the North Atlantic Ocean.

Dr. Sirpa Hakkinen, Goddard Space Flight Center, developed the model. Thank you Sirpa for your collaboration.

Jim O'Brien
Robert O. Lawton Distinguished Professor
Florida State University

# ABSTRACT

Basin-wide and regional decadal variations in the North Atlantic are investigated using the output from a prognostic coupled ice-ocean model. The study is divided into two parts. The basin-wide decadal variation in the North Atlantic is discussed in Chapter 2, and the decadal variation of the convective activity in the Labrador Sea, especially focused on the contribution of preconditioning, is discussed in Chapter 3. In this chapter, it is also shown how the convective intensity is modified and is linked to the basin-scale oscillation. Both of the phenomena involve the dominant role of the temperature variations. Chapters 2 and 3 are intended as separate reports and therefore contain their respective introductions and conclusions. The general conclusion in Chapter 4 draws together the results of this entire study.

In the North Atlantic there exist 12-14 year or quasi-decadal oscillations. Temperature anomalies that represent the upper heat content anomalies circulate around the North Atlantic basin at these timescales. It is shown from the model resutls that the Thermohaline Circulation (THC) is a central component in inducing the 12-14 year basin-wide oscillations. Responding to the changes in the THC the horizontal circulations adjust to a new oceanic state. During this transition, wave dynamics in the form of Rossby waves and advection/propagation along the western boundary play a role, influencing the horizontal circulations.

The basin-wide phenomenon suggests the important role of the convection process in the region of deep-water formation that is a driving source of the THC. In the following study, the dynamics of the decadal variability of the convective activity in the Labrador Sea is discussed. The mixed-layer depths (MLD) in the convective region show a clear decadal oscillation. It turns out that most of the variability in the MLD is accounted for by a simple mathematical model. Various analyses using the simple model lead to a conclusion that oceanic stratification before the convection more significantly contributes to the convective activity than the atmospheric forcing over the region of interest. The oceanic stratification is strongly controlled by the anomalies in the upper ocean heat transport which are advected/propagated from the subtropics as part of the basin-wide oscillations. This may indicate that the decadal oscillations are the ocean-only mode.

# 1. Introduction

The North Atlantic is a dynamically interesting part of the world ocean. In particular, the dynamical processes involving the thermohaline circulation (THC) in the Atlantic communicate with the other oceans across the globe. The recent issues of global warming and climate change have drawn much attention to the North Atlantic Ocean since this ocean is crucial for the forcing mechanism for the THC (IPCC, 2000). Many numerical (Grötzner et al., 1998; Häkkinen, 1999) and observational (Deser and Blackmon, 1993; Sutton and Allen, 1997; Mizoguchi et al., 1999) studies indicate that the North Atlantic exhibits 12-14 year oscillations in such parameters as temperature and salintiy. Temperature increase directly impacts the sea-level rise by contributing to the thermal expansion (IPCC, 2000). Indirectly it modifies the amount of sea ice that melts into freshwater, which secondarily alters the THC and may lead to global climate change (Mauritzen and Häkkinen, 1997).

In the light of the 12-14 year fluctuation, it has been under debate whether this oscillation is derived and maintained from the system that involves the air-sea coupled or ocean-only mode. Grötzner et al. (1998) in their model study explained the physical mechanism of the quasi-decadal oscillations as the delayed feedback of the Gulf Stream, whose signals are carried by the mean currents and the modification of the gyral strength through anomalous windstress curl. This is a counterpart hypothesis in the North Atlantic of the North Pacific first pro-

posed by Latif and Barnett (1994). The interdecadal mode found in a coupled model by Delworth et al. (1993) resulted simply in an ocean only mode which was excited by the stochastic atmospheric forcing, analogous to the box model experiment of Griffies and Tziperman (1998). Frankignoul and Hasselmann (1977) showed using the mixed layer model that the decadal variability in the sea surface temperature (SST) anomalies was forced by the atmospheric white noise. Following their idea, Saravanan and McWilliams (1998) demonstrated that a simple coupled model of advective thermal ocean and white noise atmosphere induced a quasi-decadal spectral peak, where the variability at these timescales also depended upon the parameter choice in the advection speed of the ocean surface temperature.

Advection/propagation of the temperature anomalies seems to play an important role in determining the timescales of the low-frequency variations and transmitting the signals to distant locations. Hansen and Bezdek (1996), using observational data, studied the advecting features of the sea surface temperature (SST) anomalies. The warm and cold anomalies propagated around both the subtropical and the subpolar gyre circulation. In the subtropics, Häkkinen (2000) showed that anomalies of the averaged temperature over the upper 1000 $m$ in her model result propagated westward from the eastern boundary. It took the anomalies about 4-7 years to cross westward across the Atlantic basin. Another example of the advective temperature anomalies was discussed by Sutton and Allen (1997). A series of warm and cold anomalies propagated along the Gulf Stream and the North Atlantic Current (NAC) eastward and poleward. The observed advecting/propagating SST features seem to be manifested in

numerical ocean modeling experiments that exhibit decadal oscillations under steady forcing with mixed surface boundary conditions (Weaver and Sarachik, 1991). Temperature and salinity anomalies were advected between the subtropical and subpolar gyres eastward and poleward. The anomalies originated from the region of deep-water formation. Furthermore, the oscillation was characterized by the unstable fluctuation of the THC between two states. Observational evidence found in the SST anomalies was shown by Mizoguchi et al. (1999), in which warm and cold anomalies alternately propagated from the Labrador Sea eastwards with a 14 year period. This suggests that variability in the horizontal circulation seems to be associated with that in the THC through the region of deep-water formation. An observational study by Deser and Blackmon (1993) showed that a basin-wide decadal oscillation found in the SST anomaly is led by the fluctuation of sea ice concentration in the Labrador Sea region, which is a forcing region for the THC, and may support an idea that the THC initiates the variability of the horizontal circulation.

A numerical experiment by Mauritzen and Häkkinen (1997) showed that the freshwater carried over from the Arctic considerably contributed to the change in the amount of the transport in the meridional overturning cell (MOC). It may be possible that the decadal oscillation in the system is completely altered due to the change in ice. The interdecadal fluctuation found in a global coupled ice/ocean/atmosphere model was attributed to the variations of ice export from the Arctic to the North Atlantic (Holland et al., 1999). The variations in the ice export and overturning circulation were associated with the surface temperature and salinity conditions south of Greenland and in the Labrador Sea region. The

decadal modes found in the above model studies appear to be predominantly driven by a convective mechanism.

Before discussing the dynamical process of convection at the decadal timescales, it is necessary to understand how it occurs at very short timescales because the physical interpretation at the shorter timescales can directly be applied to the longer timescales. At the short timescales the convection process in the open ocean is triggered by winter storms and then exchanges large volume of water masses between the surface and the intermediate or deep ocean (Marshall and Schott, 1999). One of the interesting aspects of the THC is the huge disparity between the limited size of sinking regions, which are known to be located in the Labrador, Greenland, Weddell and Mediterranean Sea, and much larger area by upwelling in the lower latitude ocean (Marshall and Schott, 1999). Convection in these regions feeds the thermohaline circulation. Warm, salty water that is driven poleward becomes dense, due to the surface cooling in the subpolar region, and then sinks to greater depths and flows equatorward. Gascard (1978) and Killworth (1983) suggested that the convection process includes three different phases such as "preconditioning" on the large-scale in order of 100 $km$, "violent mixing" on the scale of 1 $km$ and "sinking and spreading" on the scale that involves the baroclinic eddies and stratification processes. The oceanic state in the preconditioning stage contributes greatly to determining how deeply the ocean mixing can reach. Observational evidence regarding the convection process, in particular the intensity during the violent mixing that controls the volume of water masses at the decadal timescales, is limited except for few works (Dickson et al. (1996); Houghton (1996)). One

way to predict the dynamical aspect in the convection processes is through a numerical simulation. While the three phases mentioned above significantly involve the non-hydrostatic processes such as overturning of the water columns and baroclinic eddies it is realistic to parameterize the small-scale phenomena by using an enhanced vertical diffusion scheme (Klinger et al., 1996).

The scope of this study is to attempt to simulate the 12-14 year oscillation which originates from the variability in the THC and is significantly controlled by the amount and property of water masses that sink through the convection process in the region of deep-water formation. The evolution in time is first introduced to show how the information associated with the changes in the THC is imparted horizontally to the domain of influence through the Rossby wave propagation and the advection. The Rossby waves play a transmitting role between the horizontal and the meridional circulation. A prognostic coupled ice-ocean model, using a turbulence closure scheme, reconstructs the ocean field in both the Arctic and the North Atlantic. Coupling the ocean model with an ice model is necessary due to the possibility that the THC, which is a central component of the decadal oscillations, is strongly altered by the presence of freshwater from ice melt. The combined domain between the two oceans allows one to understand the physical characteristics of the basin-wide oscillation.

# 2. Basin-wide Decadal Variation in the North Atlantic

## 2.1 Abstract

The basin-wide decadal variability in the North Atlantic is investigated using forty-three years of model output from a prognostic coupled ice-ocean model that simulates both the Arctic and Atlantic Ocean. The subdomain of interest extends from $100°W$ to $20°E$ and $0°N$ to $70°N$. Empirical Orthogonal Function (EOF) analysis and two dimensional propagating complex EOF (CEOF) analysis of the upper 500 $m$ heat content indicate that there exist anomalies propagating westward from the eastern boundary in the subtropics, poleward along the western boundary to the subpolar region. It takes anomalies 13.3 years to complete one decadal cycle.

It is shown in the following order that the basin-wide decadal oscillations, which involve both the meridional overturning and the horizontal circulation, are associated with the changes of the Thermohaline Circulation (THC). The THC change is interconnected to that of the gyre-scale horizontal barotropic circulation. The gyre-scale changes seem to be introduced by altering the stratification pattern, which may be carried out by the participation of Rossy wave propagation in the mid-latitudes that is found in the heat content field. The variation of the meridional overturning cell, which is a representative of the thermohaline circulation (THC), is highly correlated with that of the meridional heat transport at $30°N$. It is also suggested that the overall oscillations

are primarily induced by the variations of the heat transport.

## 2.2 Introduction

The North Atlantic is a particularly important ocean from the climate point of view, where the surface water sinks to the deeper layer through the convection process in the subpolar region. Changes in the amount and property of the sinking waters in this region induces the oscillatory behavior in the strength and structure of the Thermohaline Circulation (THC). Due to its slow adjustment process the THC plays one of the central roles in the low-frequency variability at the timescales longer than a decade. It is naturally expected that information associated with the changes in the THC is imparted horizontally to the domain of influence through the geostrophic and Rossby adjustment processes. Weaver and Sarachik (1991) demonstrated using a numerical model with mixed boundary conditions that temperature and salinity anomalies propagated horizontally at the decadal timescales from the region of deep-water formation.

Along with the meridional circulation, the horizontal circulation plays an important part of the decadal cycle. The variations of the temperature anomalies in the North Atlantic show basin-wide quasi-decadal oscillations. Deser and Blackmon (1993) investigated the variability in the observed sea surface temperature (SST) anomaly over the whole domain, using the stationary Empirical Orthogonal Function (EOF) analysis technique. The second mode of their analysis had a dipole pattern with one sign east of Newfoundland and the opposite polarity along the southeast coast of the United States mainly along the western boundary current region. The spectral peak in the temporal function indicated 12-14 year fluctuations. Molinari et al. (1997) found evidence of

the quasi-decadal oscillation in the subsurface ocean in the subtropics.

Extending Deser and Blackmon (1993)'s work, Hansen and Bezdek (1996) demonstrated the advecting/propagating features of the SST anomalies. The warm and cold anomalies propagated following both the subtropical and the subpolar gyre circulation. Their work indicated the close link between the temperature variations and the gyre-scale circulations. Häkkinen (2000) suggested in her model result that there were propagating anomalies in the 1000 $m$ heat content, as the form of Rossby waves in the mid-latitude band $22°N$-$28°N$, that appeared in the eastern boundary and crossed the Atlantic taking about 4-7 years. Additional observational evidence of the propagative nature of the temperature anomalies was shown by Sutton and Allen (1997). A series of warm and cold anomalies propagated along the Gulf Stream and North Atlantic Current (NAC) eastward and poleward. An average velocity of the anomalies was estimated as $\sim 1.7\ cm\ s^{-1}$. The SST power spectrum averaged along the path exhibited a quasi-decadal spectral peak at 12-14 years. The temperature anomalies originated off Florida and took approximately 8-9 years to travel to the subpolar region. Horizontally advecting/propagating features indicate important dynamical processes in terms of imparting and linking decadal singals to the distant.

Häkkinen (1999) first realized that the quasi-decadal variability in the North Atlantic may be associated with the variations of the THC. She analyzed her 43-year ocean model simulation for the period 1951-1993 with a focus on the meridional heat transport (MHT) as a proxy for the strength of Meridional Overturning Cell (MOC) at $25°N$. The surface heat flux is related to the MOC

at the decadal timescales. She also tried to show the link of the THC variations to the horizontal evolution in the upper 1000 $m$ heat content, in order to understand the active involvement of the MHT or MOC related to the horizontal circulation. The cross-correlation analysis between the heat flux and upper heat content suggested that the horizontal propagating features are linked to the heat flux variations in the subpolar region. In her analyses, however, the spatial evolution associated with the changes in the THC was not systematically demonstrated.

The volume transport of the Gulf Stream was roughly 30 $Sv$ weaker in the 1970-1974 pentad than in the 1955-1959 pentad, according to a diagnostic calculation by Greatbatch et al. (1991) who performed on the hydrographic dataset in the North Atlantic. About 20 $Sv$ reduction of the northward volume transport was attributed to the weakening of the horizontal barotropic circulation in the subtropical gyre. The remaining 10 $Sv$ was due to a weakening of the cyclonic gyre in the continental slope region south of Atlantic Canada and north of the Gulf Stream. A more detailed analysis decomposes the transport variability into the wind-driven term and the term influenced by the stratification coupled to the presence of topography, so called "the Joint Effect of Baroclinicity And Relief ($JEBAR$)" (Holland and Hirschman, 1972). Quantitatively, it turned out that the $JEBAR$ term dominates the variation in the volume transport at the decadal timescales. This may indicate that the THC changed the amount of volume transport through the $JEBAR$.

Häkkinen (2001) carried out three numerical experiments, in which the basic monthly climatological surface forcing is altered by adding the following anoma-

lies: anomalies in wind and thermal forcing ($E1$), anomalies in thermal forcing only ($E2$) and anomalies in windstress forcing only ($E3$). Comparisons between experiments $E1$ and $E2$ indicated that the variations of the vertically integrated stream function are highly correlated with those of the MHT, a proxy of the MOC, and that the horizontal stream function is dynamically linked through the temperature variations. The result from $E3$ supported that the wind component does not significantly contribute to the decadal oscillations as shown by Greatbatch et al. (1991).

As for the $JEBAR$, in order to induce the variations in the depth integrated volume transport, the structure of the stratification must be altered particularly in the mid-latitudes. We expect that the changes in the stratification result from the Rossby propagation from the eastern boundary, as Häkkinen (2000) found above in the upper 1000 $m$ heat content in her model results. The role of the Rossby waves may be made clear from the relation between the barotropic circulation and the heat transport.

In this study, the basin-wide variations in the heat transport are first examined to show that the advecting/propagating anomalies mentioned above actually exist in this parameter. Here, we define the horizontal heat transport as the upper 500 $m$ heat content. Considering the timescales at which the decadal oscillations exist in the horizontal space, the decadal signals are composed of the vertical second mode. The vertical second mode is more accurately described by taking into account the upper 500 $m$ heat content, instead of the 1000 $m$ heat content as shown by Häkkinen (2000). Observational evidence by Molinari et al. (1997) indicated that the surface temperature signals along the western

boundary region are traced at least to the 400 $m$ depth, which is a maximum depth Expendable Bathythermographs ($XBT$s) can measure. As will be shown later on in Chapter 3, the temperature variations near the upper ocean play an important role in controlling convection in the Labrador Sea. It is also shown that the variations in the barotropic circulation are associated with the THC changes by alteration of the stratification pattern, which is introduced by the Rossby wave propagation in the subtropical gyre. The generation of the Rossby waves in the context of the decadal oscillations is considered to be associated with the variations of the THC. The scope of this study is to demonstrate that the decadal oscillations consist of both the horizontal and meridional circulations due to the variability of the THC.

The model and data are described in section 2.3. The method regarding the complex EOF analysis is shown in section 2.4. Results from the data analysis using the heat content and the stream function are demonstrated in comparison with each other in section 2.5. The summary and discussion follow in section 2.6.

## 2.3 Model description and output

### Model description

The coupled ice-ocean model is hydrostatic, Boussinesq and uses the sigma-coordinate system as described in Blumberg and Mellor (1987). The Level 2.5 turbulence closure scheme of Mellor and Yamada (1982) is used to determine the vertical mixing coefficients for momentum and scalar variables. When the stratification is unstable it simply makes the vertical diffusivities large to remove the unstable stratification. For the heat exchange the bulk formulation is

adopted where the heat fluxes are a function of the oceanic surface quantities. The heat exchange with a drag coefficient of $1.3 \times 10^{-3}$ is used regardless of air-ocean stability conditions (Häkkinen, 1999). The surface humidity is computed from model generated surface temperature with 95 % saturation. The model SST is also used in the upward long-wave radiation. The variability of the salinity in this model is calculated solely by dynamical processes such as advection, mixing and sea ice import. The dynamic-thermodynamic ice model is coupled to the ocean model via interfacial stresses and via salinity and heat fluxes through the ice-water interface. The ice model uses a generalized viscous rheology, as discussed by Häkkinen and Mellor (1992). Note that the surface boundary conditions used in this model are not the mixed boundary conditions as mentioned in the 2.2 introduction. The model extends from the Bering Strait to 15°S with resolution of 7/10° in longitude by 9/10° in latitude in a rotated curvillinear coordinate system. There are a total of 20 sigma-levels in the vertical with higher resolution near the surface. The transports at oceanic lateral boundaries are specified to be 0.8 Sv through the Bering Strait, and 0.8 $Sv$ out at 15°S. At the southern boundary the salinities and temperature are relaxed to Levitus values in 5 grid rows from the boundary. Restoring of T and S is also used at the Mediterranean outflow point. This model is forced with modern atmospheric data in order to make the model fields as realistic as possible with an emphasis on the high latitude simulation due to the ice dynamics. The model is forced with atmospheric climatological data for the first 10 years, after which the COADS anomalies are added to the atmospheric climatologies. Only the cloudiness field, the precipitation minus evaporation $(P - E)$ field and the

river runoff continue to be climatological. For the detailed description of the model, readers are referred to Häkkinen (1999).

### Model output

A 43-year subset of model output from a prognostic coupled ice-ocean model covering the North Atlantic from $0°N$ to $70°N$ and from $100°W$ to $20°E$ from 1951 through 1993 is examined. The upper 500 $m$ heat content and vertically integrated stream function from surface to bottom are utilized to investigate the spatiotemporal variabilities in the Atlantic basin at the quasi-decadal timescales. The stream function is obtained by integrating the velocity field, which is horizontally non-divergent. Both of the parameters are Hanning-filtered six times in space in order to make the horizontal field smooth enough to emphasize the decadal signals. The monthly climatology fields are calculated by averaging all the months in time at each location. The anomalies used in the calculation are the differences from the their respective climatology. The Meridional Heat Transport (MHT), used in comparison with the stream function, is computed by integrating both vertically and horizontally the product quantity, that is, velocity multiplied by the temperature fluxes at arbitrary latitudes.

## 2.4 Method

### Two dimensional propagating complex empirical orthogonal function (CEOF)

For the analysis of the heat content anomalies in particular, two dimensional propagating complex empirical orthogonal function analysis (CEOF) (Barnett, 1983; Horel, 1984; Shriver et al., 1991; Sharp, 1996; Mizoguchi et al., 1999) is used in this study to extract physical information on propagating features from

the upper 500 $m$ heat content at the quasi-decadal timescales. The domain is on a 150 $\times$ 142 grid, where there are 6472 spatial points in the ocean and 14828 land points set. The monthly anomaly timeseries at each ocean point are low-pass filtered using a 4-year running mean. The timeseries of anomalies are quadratically detrended to remove much longer timescales. The variable $u(x_m, t) = \mathrm{SST}(\mathbf{r}_m, t)$, where $\mathbf{r}_m$ is the position vector and $t$ is the time index, can be written

$$u(x_m, t) = \sum_{\omega} [a_m(\omega) cos(\omega t) + b_m(\omega) sin(\omega t)] \tag{1}$$

where $a_m(\omega)$, $b_m(\omega)$ are the Fourier coefficients. Define the complex representation of a variable as

$$U_m = \sum_{\omega} c_m(\omega) e^{-i\omega t} \tag{2}$$

where $c_m(\omega) = a_m(\omega) + ib_m(\omega)$.

The expansion of (2) gives

$$U_m(t) = \sum_{\omega} \{[a_m(\omega) cos(\omega t) + b_m(\omega) sin(\omega t)] + i[b_m(\omega) cos(\omega t) - a_m(\omega) sin(\omega t)]\}$$
$$= u_m(t) + i\hat{u}_m(t) \tag{3}$$

The imaginary part $\hat{u}_m(t)$ is the Hilbert transform of the real part, which is in fact a $\pi/2$ shifted function of the real part in time with the same magnitude of the Fourier transform.

The variable $U_m(t)$ is represented as a complex-valued spatio-temporal matrix. $U_{m,t}$ is formed so that each row of the matrix is a temporal array, and each column is a spatial array, where $m = 1, 2, ..., M$, $t = 1, 2, ..., N$, and

$M = 6472$ (ocean points), $N = 468$ (months). The covariance array is calculated by multiplying the $M \times N$ matrix by its transpose to form a $N \times N$ Hermitian matrix which is symmetric with real-valued diagonal elements. By solving the eigensystem equation of the covariance matrix, the eigenvalue vector $\lambda_i$, where $i = 1, 2, ...N$, and the spatial and temporal functions (eigenvectors) are obtained. Normalized eigenvalues represent a relative variance of the original data set $(\lambda_i(\sum_{i=1}^{n} \lambda_i)^{-1})$.

The data $U_m(t)$ are reconstructed by the summation of spatial (SF) and temporal functions (TF) as follows:

$$U_m(t) = \sum_l [S_l(m)e^{i\theta_l(m)}]^*[R_l(t)e^{i\phi_l(t)}] \tag{4}$$

where $SF = S_l(m)e^{i\theta_l(m)}$ and $TF = R_l(t)e^{i\phi_l(t)}$, respectively and $m$ and $*$ denote a spatial index and a complex conjugate, respectively.

The spatial amplitude function $S_l(m)$ is defined as

$$S_l(m) = [(SF)(SF)^*]^{1/2}. \tag{5}$$

The spatial phase function $\theta_l(m)$ is defined as

$$\theta_l(m) = \arctan[Im(SF)/Re(SF)]. \tag{6}$$

The wave number $\mathbf{k}$ is obtained by

$$\mathbf{k} = \frac{\partial \theta_l(m)}{\partial \mathbf{x}} \tag{7}$$

where $\mathbf{x}$=$(x, y)$.

The temporal amplitude function $R_l(t)$ is

$$R_l(t) = [(TF)(TF)^*]^{1/2}, \tag{8}$$

the temporal phase function $\phi_l(t)$ is

$$\phi_l(t) = \arctan[Im(TF)/Re(TF)], \tag{9}$$

and the frequency $\omega$ is calculated from the temporal phase function as

$$\omega = \frac{\partial \phi_l(t)}{\partial t}. \tag{10}$$

### 2.5 Results

#### Upper 500m heat content

The quadratically detrended and lowpass filtered datasets from the upper 500 $m$ heat content and the stream function are analyzed using the stationary EOF and the propagating complex EOF analysis techniques to show how they are related at the quasi-decadal timescales.

The data field from the upper 500 $m$ heat content is first annually averaged to form the anomalies and quadratically detrended, after which the timeseries are binomial-filtered once to extract the decadal signals. The standard deviation from the average over the 43 years during the period from 1951 to 1993 (Fig. 1 (a)) shows the strong variations along the Gulf Stream and the Labrador Sea region, with less variation along $20°N$ extending across the ocean basin. The Empirical Orthogonal Function (EOF) analysis technique (Jolliffe, 1986) is performed in order to extract the dominant standing patterns in the data field. The EOF analysis technique decomposes the data fields into real orthogonal pairs of the resulting spatial ($SF$) and temporal ($TF$) patterns. The product of the resulting spatio-temporal functions reproduces the major stationary patterns of the analyzed datasets. The variances of the leading four modes account for 24.5 %, 16.7 %, 12.2 % and 8.6 % of the total variance, respectively. The opposite

signs of the temperature anomalies are divided between the east and west as the standing mode in the spatial function of the first mode (Fig. 1 (b)). It is suggested that the pronouced changes exist off the African coast and along the Gulf Stream and Labrador Sea region. The temporal function of the leading mode (Fig. 1 (c)) shows the clear quasi-decadal oscillations that fluctuate with an amplitude of 0.3 $^{\circ}C$. In fact, the positive and negative phase in the timeseries roughly coincide with the pentad in 1955-1959 and in 1970-1974, respectively, as defined in the analysis by Greatbatch et al. (1991).

The autocorrelation function of the heat content mode 1 is used to examine whether there are any cyclic patterns in the field. The other modes do not contain the evidence of the cyclic patterns. Autocorrelation of the first mode exhibits the largest negative correlation roughly at 6-7 year lag with a correlation coefficient less than -0.6 (Fig. 1 (d)), suggesting a cyclic phenomenon in the heat content mode 1 with a period of 12-14 years. Häkkinen (2000) showed that the anomalous fields in the upper $1000m$ heat content had propagating features, which were extracted by lag cross-correlating the timeseries between the first and the second mode that were obtained from the EOF decomposition.

**CEOF mode 1 of the heat content**

The EOF analysis (Fig. 1) suggests that there are propagating features in the mid-latitude ocean in the heat content at the quasi-decadal timescales. Another way to see the propagating features is by using two dimensional propagating complex EOF analysis (see the Method section). Unlike the stationary EOF analysis it seems that longer timeseries than the annual average are needed, so that the CEOF analysis can separate the physical propagating modes. Instead

of annually averaged data, the monthly values from 1951 to 1993 are 4-year lowpass filtered and submitted to the CEOF calculation. This way, the matrix manipulation is performed more efficiently. In this section, only the behavior of the first mode is discussed which contains the quasi-decadal patterns.

The spatial amplitude function for the first mode of CEOF (CEOF1) (Fig. 2 (a)) has the maxima along the Gulf Stream and the Labrador Sea. These are the regions where the most pronounced signals are found during the cycle. Both the real and imaginary parts of the timeseries (Fig. 2 (b)) show the quasi-decadal variability that fluctuates with a period of approximately 14 years. Since the argument of the phase function is defined from 0° to 360° the timeseries of the function cannot be plotted as a continuous function. Therefore, it is defined from 0° to 1500° to make it continuous (Fig. 2 (c)). In Fig. 2 (c), the dotted line is the temporal phase function obtained from the CEOF mode 1. The solid line is the best fit to the functions; $a$ is a $y$ intersect and $b$ is the slope of the best fit function. $y = a + bx$ represents the linear function. The $x$ axis is a time axis from 1953 to 1991 and the $y$ axis is an argument of the phase functions in degrees. The reciprocal of the slope is a period of one cycle. The $y$ intersect has the value of 111.403°. The linear fit is applied to this function so that the fundamental period $\omega$ is estimated. The period of mode 1 is about 13.3 years, which has been roughly suggested by the autocorrelation in the previous section (lag = 6 years). The temporal evolution of the spatial field is obtained by multiplying the spatial and temporal function of the first mode [as in Eq. (4)] and taking the real component. The reconstructed spatial patterns for the heat content anomalies for CEOF1, half the cycle from 1957 to 1964, are

shown in Fig. 3. The sequences of the annual averages are selected because they show relatively strong signals compared to other sets of the half period. The propagating features are barely detected from the mid-1960s to mid-1970s, probably due to the orthonormal constraints.

In 1957, warm anomalies are located off the African and European continents around the $20°N$ to $50°N$ latitude band. The anomalies propagate westward across the basin. The warm anomalies that reach the western boundary begin propagating along the Gulf Stream region to the north. The anomalies are enhanced while progressing to the north along the east coast of the U.S. Eventually, they reach the Labrador Sea region and immediately spread afterward. Häkkinen (2000) speculated that the anomalies along this region are reinforced by the air-sea coupling through the heat flux. The speed of the warm anomaly along the western boundary is estimated as $O(2.0)\ cm\ s^{-1}$. The anomaly is followed from 1961 to 1964 while it moves from $20°N$ to $55°N$. The cold anomaly roughly follows the same path with the similar speed. Sutton and Allen (1997) showed propagting SST anomalies with a speed of $\sim 1.7\ cm\ s^{-1}$ along the Gulf Sream and NAC at the quasi-decadal timescales in their observational data. The estimated power spectrum averaged along the path exhibited variations of these timescales. The pronounced warm anomalies along the western boundary region seen in the CEOF reconstruction is the largest contributor to the MHT or the MOC.

### Cross-correlation analysis between the upper 500 $m$ heat content and the stream function

Lagged cross-correlations between the two parameters are calculated to explore the relationship between the heat content anomalies and the anomalous gyre circulation. The high negative correlations indicate the spatial evolution with respect to the time before the extrema in EOF 1 in the stream function is achieved. The timeseries previously obtained from the heat content and the stream function EOF mode 1 are annually averaged in order to make the calculation computationally inexpensive instead of using the monthly values. The annual averaging does not make any significant change in the timeseries variations because they have been 4-year lowpass filtered.

Only the evolution of the negative values is described in Fig. 4, prior to the 0 lag year, in order to focus the process that contributes to changes in the gyre-scale variability. At a lag of -7 years the negative anomalies appear along the eastern boundary. At a -5 year lag the negative anomalies start propagating westward from the eastern boundary. The propagating features in the eastern boundary region do not exsit at all in the spatial function (Fig. 5 (a)) of the stream function mode 1, whereas the reconstructed field from the CEOF mode 1 in the heat content anomalies contain robust anomalies that are located off the African continent at the similar latitudal band as in the cross-correlation analysis. It is speculated that in spite of the feasible signals that are situated in the eastern half of the domain the timeseries of the 1st mode stream function are highly correlated with those in the heat content anomalies in the same region. During the subsequent years until no lag year the cold anomalies keep moving

toward the western boundary region in the subtropical gyre and change the gyre-scale circulation. They are dominantly present in the heat content field. It is suggested that prior to the large-scale circulation changes there already existed heat content anomalies in the eastern ocean domain. They are a potential candidate to produce and maintain the decadal oscillations of the barotropic transport via the *JEBAR*.

**Relation between meridional heat transport and vertically integrated stream function**

In this section, the meridional heat transport and the vertically integrated stream function are compared to examine the relation between the two. Following Häkkinen (2001)'s analysis, the monthly dataset from the stream function is 4-year lowpass filtered and binomial filtered once. The filtered data field is submitted to the stationary EOF to extract the standing spatial patterns. The variance of the first mode accounts for 51.8 % of the total variance and the discussion is focused on only the first mode since the primary mode of the decadal oscillations resulted from the thermal component mode. The spatial pattern of this mode (Fig. 5 (a)) has a dipole strucutre with one polarity in the Labrador Sea and along the east coast of the U.S. and the opposite polarity in the subtropical gyre and the Gulf Stream region. The eastern half of the domain shows the spatial pattern with very small variance. The temporal function of this mode shows clear 12-14 year variability.

The timeseries in the EOF mode 1 from the stream function is highly correlated with that from the MHT ($r = 0.80$ at 0 year lag) at low-frequencies (Fig. 5 (b)). A numerical model experiment from Sarmiento and Bryan (1982) showed

that MHT in the latitude band $20°N$ to $30°N$ in the North Atlantic consists primarily of the overturning cell (MOC), suggesting that the variability in the gyre-scale circulation results from that in the MOC through the temperature changes. A model result by Häkkinen (1999) (in her Fig. 5) showed that the MHT is a proxy for the strength of MOC at $25°N$ at the decadal timescales. The primarily thermally-driven MOC or MHT and the 1st mode stream function are interconnected.

As described in the heat content field, the subtropical region is characterized by the dominant features of the Rossby wave propagation. Before the pronounced signals along the western boudary region appear there already existed heat content anomalies in the eastern ocean domain in the $20°N$ to $30°N$ latitudal band. The $JEBAR$ seems to play a dominant role in the decadal oscillations as seen in the 1st EOF mode of the stream function. For the $JEBAR$ to be established it is necessary that the changes in the stratification pattern in the subtropical gyre are introduced somehow. The change in the gyre-scale stratification pattern is tightly connected to the arrival of the Rossby waves originating from the eastern boundary to the western North Atlantic. The Rossby waves, induced at the eastern boundary associated with the THC variations, propagate westward and arrive near the western boundary, where the change in structure of the stratification causes the barotropic volume transport by the presence of the topography ($JEBAR$).

## 2.6 Summary and conclusion

In this study, the variability of the basin-wide quasi-decadal oscillation has been investigated. The scope of the study is to show that the basin-wide decadal os-

cillations, which involve both the meridional and horizontal circulations, are associated with the variations of the Thermohaline Circulation (THC). First of all, the upper 500 $m$ heat content is used to demonstrate that there exist 12-14 year oscillations in this field and they are characterized by the advecting/propagating features. The statistical techniques such as stationary EOF and two dimensional propagating complex EOF (CEOF) analyses are performed to separate the data fileds into dominant physical modes. The auto-correlation analysis applied to the heat content anomaly field suggests the data have propagating features with a period of 12-14 years. Supporting the propagating nature of the anomalies, the first mode of the CEOF clearly shows the evidence of the propagating signals with an estimated period of 13.3 years. The pronounced decadal signals in the upper heat content propagate northward along the Gulf Stream and the North Atlantic Current, reach the subpolar gyre, and then immediately spread afterward. The heat transport in the upper ocean dominates the decadal oscillations in the horizontal component.

Cross-correlations among the MHT, horizontal heat content and horizontal barotropic volume transport have revealed that the THC and horizontal circulations are tightly interconnected in that the change in the THC induces the decadal oscillations and the horizontal circulations also exhibit the oscillatory nature through the adjustment processes. The relations between the horizontal heat transport and the vertically integrated volume transport suggest that the oscillations initiated by the THC are imparted in the horizontal directions through the temperature variations that alter the structure of the stratification and in turn the integrated volume transport, in which remotely excited Rossby

waves participate. The Rossby wave propagations seem to be associated with the THC changes and relay the signals back to the THC.

In the light of the decadal oscillations found in the THC, Häkkinen (2000) proposed a potential air-sea coupled mode, which is linked through the heat flux. In fact, the northward propagating anomalies along the western boundary seem to be somehow enhanced while advancing to the subpolar region, as shown in Fig. 3. She also speculated that the air-sea coupling exists in the region of deep-water formation since the sinking water masses form through the convection process, which is strongly linked to the atmospheric cooling. The change in the volume of the sinking water results in the strengthening and weakening of the Meridional Overturning Cell (MOC). This strongly suggests that driving mechanism for the decadal oscillation may exist in the Labrador Sea region, which leads to the more focused study in the following section, specifically in terms of the intensity and nature of the convection. Finally, it should be mentioned that the quasi-decadal oscillation found in this model study is attributed to the forcing fields that implicitly include the air-sea coupling therein. Therefore, the oscillation is not a kind of solution resulting from the mixed boundary conditions as mentioned in the introduction. Such a simple numerical model that it is forced with the 12-14 year period may give an explanation how the decadal mode is generated and maintained, which may lead to future study.

# 3. Decadal Variability of the Convective Activity in the Labrador Sea: Contribution of the Preconditioning

## 3.1 Abstract

The decadal variability of the convective activity in the Labrador Sea is investigated using forty-three years of model output from a prognostic coupled ice-ocean model that simulates both the Arctic and the Atlantic Ocean. The subdomain of interest extends from $60°W$ to $40°W$ and $45°N$ to $65°N$. The surface density field and the mixed-layer depth indicate that a quasi-decadal oscillation exists in the convective site that is located along the continental slope, off the eastern Labrador coast.

The selection of the convective site and its intensity in March are associated with the oceanic state at the preconditioning stage in the previous November. The doming of the isopycnals near the surface determines the depth of vertical mixing during the violent mixing phase of the convective process. A simple analytical one-dimensional model reproduces most of the variability of the convective activity in the region of deep-water formation. The analytical model computed with variability only in the ocean suggests that the convections at the decadal timescales are subject to changes in the upper ocean stratification. In addition, the oceanic density structure is dominantly controlled by the temperature variations.

Basin-wide decadal oscillations in the North Atlantic seem to influence the variability in the Labrador Sea. This region plays a key role in terms of the

variation in the THC, which is a central component of the basin-wide quasi-decadal oscillations and is largely associated with the temperature changes in the upper ocean.

## 3.2 Introduction

The Labrador Sea (LS) is a particularly interesting region of the ocean from a dynamic perspective. Here, the Atlantic water is ventilated at the sea surface via convection, which can significantly modify the meridional overturning circulation at the decadal timescales (Holland et al., 1999).

In Chapter 2, it has been learned that the THC is a central component of the basin-wide decadal oscillations. The THC is, to a large extent, driven by the convection process that takes place in a region of deep-water formation such as the Labrador Sea. The surface water sinks to a greater depth in this region and changes in the amount and property of the sinking water may induce variations of the THC. When the THC changes due to variations in convection, the domain of influence responds in an oscillatory manner through the geostrophic and Rossby adjustment processes. From the previous chapter, it is clear that Rossby waves propagating westward from the eastern boundary in mid-latitudes transmit information horizontally through the ocean. Arrival of the Rossby waves at the western boundary region modifies the stratification pattern there, which eventually alters the THC as the signals travel northward along the western boundary to the region of deep-water formation. The basin-wide decadal variability seems to originate in the Labrador Sea region in terms of the THC variations.

Data from Curry and McCartney (1996) showed that there is strong low

frequency variability in the Labrador Sea Water (LSW) properties such as temperature and salinity from the 1930s to the present. Thickness of the LSW layer is directly translated to the intensity of the deep convection with strong convection producing a thick layer and relatively thin layer associated with weak convection. According to the thickness of LSW, the strong convective events occurred roughly in early 1950s, 1960s, 1970s and 1990s, indicative of a quasi-decadal oscillation. These periods loosely coincided with the cooler, fresher LSW conditions. The temperature showed a long warming trend from 1930s to 1972, followed by a cooling trend that continued until the present. The variation of the surface salinity is illustrated by the appearance of the Great Salinity Anomalies in 1970s (GSA70s) and 1980s (GSA80s) (Dickson et al., 1988; Belkin et al., 1996). During those years the surface layer was occupied by extremely cold and fresh water anomalies, which affected the intensity of the convection. Curry and McCartney (1996)'s work suggests that the temporal variability in the LS seems to be controlled by the both temperature and salinity components. Considering its important implication to the climate system only few studies regarding the decadal variability in the convective intensity have been attempted (Dickson et al., 1996).

Before discussing the dynamical process in convection at the decadal timescales, perhaps it is necessary to understand how it occurs at very short timescales compared to the decadal because the physical interpretation at the shorter timescales can directly be applied to that at much longer timescales, as will be shown later on.

One of the prominent features of convection is that it occurs in very localized

regions of the northern North Atlantic. Observations (Marshall and Schott, 1999) suggested that there are certain conditions and specific locations that are common to deep-water formation. The surface water needs to be exposed to cold and dry strong winter winds to make it heavy enough to sink to the deeper water. In this sense, the open ocean adjacent to boundaries is favored, at which the preferred atmospheric conditions are always supplied from the land or ice surfaces. The weakly stratified water beneath the seasonal thermocline must be brought up to the surface, immediately after the thermocline is eroded due to the surface mixing and cooling. The doming effect of the isopycnals, situated at the center of the cyclonic circulation in the LS, sets up the condition for the weakly stratified water from the below to ventilate to the surface (LabSeaGroup, 1998).

As discussed by Killworth (1976), there are basically three different phases in the convective processes. The first is preconditioning, which is followed by violent mixing associated with surface cooling, during which vertically homogenized convective chimneys are established. Lastly, the sinking and spreading phase takes place. In the oceanic precondition, there are also three different spatial scales, i.e., plume (Send and Marshall, 1995), eddy (Visbeck et al., 1996) and gyre scales. The first two are non-hydrostatic and have spatial scales of 100 $m$ - 1 $km$ and 5 $km$ - 100 $km$, respectively. Baroclinic instability plays a major role at these scales. The gyre scale (50 - 1000 $km$) determines the large scale factors that are subject to general circulation and vertical stratification patterns.

The observations have shown that the spatial scale of a convective chim-

ney in the LS is roughly 50 $km$ (Gascard and Clarke, 1983) whereas that of atmospheric buoyancy forcing is $O(500\ km)$, one order of magnitude larger. This implies that the gyre-scale oceanic structure has something to do with the selection of a convective site, as well as the intensity of the penetration depth. The convective intensity may be already pre-determined by the oceanic preconditioned state, or determined by the combination of both the on-going buoyancy forcing and the oceanic background stratification before it. Alverson and Owens (1996) showed the importance of the surface intensified oceanic stratification for convection to deeply penetrate and compared the MLD depending upon different intensities. They also showed that a simple analytical one-dimensional nonpenetrative convection model compared well with results from a numerical model.

In this chapter the investigation focuses mainly on large-scale convective phenomena in the LS. First, attention is paid to the dynamical explanation of the convective activity at shorter timescales compared to the decadal, which later on leads to a conclusion that the controlling mechanism of the decadal convective process is tightly connected to the oceanic density stratification in the preconditioning. In addition, it will be shown that the decadal variation in the convective depth is tightly linked to the basin-wide decadal oscillations in the North Atlantic, which has been discussed in the previous chapter. The dataset consists of output from a coupled ice-ocean model covering the Arctic and North Atlantic. The coupled ice-ocean model simulates the high latitude oceans and is used to reproduce the ice export variations, which possibly affect the LS via freshwater input. For the analysis of the LS variability a subset of

the model domain is examined.

The model description and data are described in section 2, the results are shown in the context of other observations and compared to a simple analytical model in section 3. A discussion follows in section 4.

### 3.3 Model description and output

The model used in this study is the same as described in Chapter 2. Detailed model description may be found in Chapter 2. The model is a prognostic coupled ice-ocean model.

The coupled ice-ocean model is hydrostatic and it does not resolve the plume and eddy scales that are mentioned above. Even though the model does not resolve the actual small-scale convective chimneys, water mass formation takes place through vertical diffusion which is determined prognostically using a turbulence closure scheme by Mellor and Yamada (1982). The assumption of hydrostatic balance is valid when the vertical mixing process is properly parameterized. In this model, enhanced vertical diffusion with an arbitrarily chosen value of vertical diffusivity is used to parameterize convection because the hydrostatic model cannot overturn. Klinger et al. (1996) (in their appendix) showed that vertical diffusion is formally the same as "adjustment" with a finite adjustment timescale.

A 43-year subset of monthly model output such as temperature and salinity fields from the coupled ice-ocean model covering the LS from 1951 through 1993 is examined. The domain of study extends from 45°N to 65°N, 60°W to 40°W. The density is calculated from the temperature and the salinity using the International Equation of State of Sea Water (UNESCO, 1981). The forcing fields

from the COADS data sets have inherent uncertainties due to historical changes in instrumentation, observation techniques, coding methods, data density, and ship tracking. The data period for the analysis is after the large shift observed by Deser and Blackmon (1993). All the parameters on the sigma coordinate in the model are linearly interpolated to the 33 level standard depths from the surface to the 5500 $m$.

### 3.4 Results

The objective of this paper is to describe the decadal variability of the deep-water formation in the LS, specifically in the region where the deepest convection takes place (see Fig. 6 (d)). A subset of the model results is specific to the area of cyclonic circulation, inside the LS. The main focus is to investigate the variability in the LS gyre temperatures, densities and the mixed-layer depths (MLD) and show how strongly oceanic stratification governs the convective depth, using a simple one-dimensional model. Furthermore, it is shown that the decadal oscillation in the LS is tightly linked to the basin-wide oscillation.

#### Surface and subsurface variabilites

The surface density in March is chosen to investigate the convective site and its intensity. The high surface density in March is located along the continental slope, off the eastern Labrador coast (Fig. 6 (a)-(c)). Since the LS is weakly stratified, instead of the real value of the potential density ($\sigma_\theta$), ($\sigma_\theta$ - 27.00 ) $\times$ 100 is shown to present the density fields. The region of deep-water formation which is represented by 56 data points is defined shown in Fig. 6 (b) and averaged to obtain a one-point value to specify the possible convective periods and

locations. This region covers the active part of the convection that takes place in March, 1973, since most of the convection sites are located around this fixed area.

The density difference of 0.005 ($kg/m^3$) between the surface and the mixed-layer base is used as a measure of the MLD. Kara et al. (2000) introduced an optimal definition for the ocean MLD calculated from the density profile, instead of an empirical estimate. However, in this study the classical diagnostic criterion $\delta\sigma_\theta = 0.005$ ($kg/m^3$) is adopted for simplification. The MLD in 1993 with the deepest mixing is located at the center of the high surface density (Fig. 6 (d)). The maximum MLD in the LS in March indicates the convective depth. Large values of surface density correspond to the deepest convection. The heaviest density fields appear in March 1973, 1983 and 1993, suggesting that the deepest convection occurred during these years. In fact, observations (LabSeaGroup, 1998) indicated that the winter of 1993 was an active season with convection penetrating down to more than 2200 $m$ depth, which is also seen in Fig. 6 (d). Decadal variability of the convective activity in the LS is suggestive in the timeseries of MLD (Fig. 7). There is a deep-mixing event in the mid 80's just as stong as the deep ones in the early 60's, early 70's and early 90's. During the weak convection years the mixing reaches a depth of approximately 1000 $m$. The timeseries fluctuates with an amplitude of over 400 $m$ which is slightly reduced due to the spatial averaging over the region of deep-water formation. There are three weak and three strong events seen over the course of the forty-three years.

Decadal variability in the covective activity is also seen in the potential tem-

perature profile in March. The vertical temperature versus time diagram (Fig. 8) indicates the presence of convection that homogenizes the water column from the surface to variable depths depending upon the convective intensity. Colder water in the region suggests deeper penetration and the warmer the shallower. Every year the mixing reaches the depth of at least 1000m. Distinctively strong mixing events occur from 1971 to 1972 and from 1983 to 1984, reaching depths greater than 2000 $m$. The event in the early 60's is also considered as a strong event. However, it does not appear as strong. This may have something to do with a fact that the decadal oscillation is embedded in the long-term trend in the temperature field. The temperature varies from $1.9°C$ to $4.4°C$ and fluctuates at the decadal timescales with an amplitude of approximately $0.7°C$.

The timeseries of sea surface temperature anomalies (SSTA) from the coupled ice-ocean model in March, which is averaged over the region shown in Fig. 6 (b), is highly correlated to that from the SSTA in March in observational analysis by Houghton (1996) (Fig. 9) in particular after 1960 ($r = 0.84$ at 0 lag). Both timeseries are normalized to emphasize the oscillatory pattern. The period and relative amplitudes of oscillation are nearly identical in both the timeseries.

The observed sea surface salinity anomalies (SSSA) (Fig. 10) in August from Houghton (1996) also indicates the clear decadal fluctuation at the low-frequency in the LS. While the timeseries of the modeled SSTA (Fig. 9) is highly correlated with that of the observed SSTA, the timeseries of SSSA (Fig. 10) is not correlated with the observed SSSA at all (correlation coefficient not shown).

Thickness of the Labrador Sea Water (LSW) layer is directly related to the intensity of wintertime convection or mixed layer depth due to a convection,

with strong convection creating a thick layer and weak convection resulting in a relatively thin layer (Curry and McCartney, 1996). The timeseries of LSW thickness (Curry and McCartney, 1996) showed a clear sinusoidal decadal behavior. Strong convection occurred during the early 1960s, 1970s and 1990s whereas the counterpart, that appears in 1980s in the MLD timeseries in our model results, did not take place according to the LSW thickness. The temperature timeseries from Curry and McCartney (1996) showed a long warming trend from 1930s to 1972, followed by a cooling trend that continued until the present, which were different than the SSTA timeseries seen in Houghton (1996) that showed the strong temperature minimum during the early 1980s. It is plausible that evidence of the decadal oscillations is found in both the fields of the model MLD and the observed LSW thickess.

**Region of deep-water formation**

The region of deep-water formation (Fig. 6) coincides with that estimated from observations. A salinity map (Lilly et al., 1999) (their Fig. 2) on the $\sigma_0 = 27.72$ $(g\ kg^{-1})$ isopycnal during 1965-67 shows the region where the deep convection took place. The central salinity minimum, which was trapped by the encircling boundary currents and considered to be a center of convection, was located at about 51.5°W, 57°N. The second salinity minimum that was identified as 34.88 $(psu)$ extended roughly from 49°W to 56°W, 54°N to 59°N. The low salinity extension of the LSW flowed southeastward along the continental slope out of the LS domain (Pickart et al., 1997). Other observational evidence of the convective site in the LS is presented by Gascard and Clarke (1983), and Pickart (2000).

There are some features and conditions that are common in all the sites of deep convection in such places as the Mediterranean, Greenland and LS. The region of deep-water formation needs to be exposed to cold and dry strong winter winds to make the surface water heavy enough to sink. In this sense, the open ocean adjacent to boundaries are favored, at which the preferred atmospheric conditions are always supplied from the land or ice surfaces. The weakly stratified water beneath the seasonal thermocline must be brought up to the surface immediately after the thermocline is eroded due to the surface mixing and cooling. The doming effect of the isopycnals, at the center of the cyclonic circulation in the case of the LS, sets up the condition for the weakly stratified water from the below to be ready for reemerging to the surface.

In light of the domed isopycnals, the "preconditioning" stage in the convective process (see the 3.2 introduction) significantly contributes to the determination of the convective site. Observations showed that the spatial scale of convective chimneys in the LS is roughly $O(50\ km)$ whereas that of atmospheric buoyancy forcing is $O(500\ km)$, one order of magnitude larger (Gascard and Clarke, 1983). A model study by Wallace and Lazier (1988) suggested that atmospheric cooling may not be the only factor for the convection to occur since most of the vertical profiles were not favorable for overturning below 1000m under normal conditions. This implies that somehow the gyre-scale oceanic structure plays a key role for the selection of convective site as well as the intensity of the penetration depth, and that the intensity of the convection is pre-determined by the oceanic state at the preconditioning stage or determined by the combination of both the on-going buoyancy forcing and the oceanic background stratification

before the event occurs. The maximum density at the violent mixing stage in March (Fig. 11 (c) and (d)) is always located at the center of the doming at the preconditioning stage in November (Fig. 11 (a) and (b)). The doming stratification in November acts to lift and squeeze the near-surface isopycnals toward the surface. In order to convect deeply, significant cooling is first required to penetrate the strongly stratified isopycnals near the surface and then further mixing progresses rather rapidly due to the weak strafication below. Consequently, the structure of the domed isopycnals preselects a region for deepest convection. It is suggested that only after the structure of thepycnocline is organized can the buoyancy forcing select the convective site and resume the deeper mixing.

### Preconditioning

The oceanic state in November represents a precondition for convection that takes place in March in the following year. Condition before and after convection for 1965-1966 and 1983-84 are shown to illustrate weak and strong periods of convection as seen in the timeseries of MLD (Fig. 7). In November, 1983, isopycnals (Fig. 11 (b)) sharply dome up toward the center of the cyclonic gyre, lifting the stratification and squeezing the near-surface isopycnals toward the surface. In November, 1965, the doming effect of the isopycnals (Fig. 11 (a)) appears much weaker compared to that in November, 1983.

The isopycnal 27.91 ($kg/m^3$), for example, increases its height about 700m upward compared to that in November, 1965 (Fig. 11 (a)). A dense water mass of 27.98 ($kg/m^3$) (Fig. 11 (b)) appears near the bottom in 1983 while the counterpart in November 1965 (Fig. 11 (a)) shows the water mass of 27.96 ($kg/m^3$), which also indicates the lifting of the stratification. In March 1984

(Fig. 11 (d)) chimneys are established due to the convective mixing, and all the isopycnals are vertically aligned. The mixed-layer depth reaches a depth greater than 2000m in 1983 (Fig. 11 (d)), whereas it only reaches the depth of 1000m in March 1966 (Fig. 11 (c)).

There seems to be a strong link between the degree of the squeezing of the isopycnals near the surface in November and the convective intensity in March in the following year. The stronger the ocean is stratified at the near-surface the greater the depth reached by violent mixing, and vice versa. Alverson and Owens (1996) showed the effect of the squreezed isopycnals near the surface on the penetrating depth using a simple one-dimensional non-penetrative convection model with an exponential ocean stratification and the constant buoyancy forcing, whose e-folding scale is a measure of the degree to which the stratification is surface intensified. The more strongly stratified the near-surface water is the greater the depth the mixing can reach (see their Fig. 15 (d)). Their results from the analytical model also compared well to those from their numerical model.

**One-dimensional mixed-layer model**

Following Alverson and Owens (1996), the mixed-layer depth in March is diagnosed using buoyancy flux and the ocean vertical density profile at the preconditioning stage in November, just before the convection occurs. That the calculation is only a function of the vertical ($z$) and the time ($t$) is also assumed. The mixed-layer depth in March is chosen to represent the greatest depth of convection during the year. The density profile in November is selected as the preconditioning state because in some years the convective events

resume in December. For convenience, the November before the convection is considered as the initial condition for the following year. For example, the pre-condition in November 1951 is labeled as 1952. This diagnostic calculation is performed each year from 1952 through 1993.

A simple one-dimensional mixed-layer model (eq.11), that assumes only vertical dynamics, is used to estimate the depth of convection during the violent mixing stage at an arbitrary location and year.

$$B(t) = \int_{t_1}^{t_2} b(t')dt' = \frac{g}{\rho_0}\int_0^d (\rho(d,t) - \rho(z,t))dz \tag{11}$$

where $d = d(z,t)$ is a MLD to be estimated from the above equation, $B(t)$ the surface buoyancy, $b(t)$ the surface buoyancy flux, $g$ the gravity, $\rho_0$ the mean density, $\rho(z,t)$ the initial background stratification in November and $\rho(d,t)$ the uniform density profile mixed to the depth $d$.

The MLD is calculated from buoyancy in two-dimensional space and time (Fig. 12). The coupled ice-ocean model calculates the heat and salinity fluxes using the oceanic surface conditions. The buoyancy flux is computed from the heat and salinity fluxes. Buoyancy fluxes are integrated over the period from November ($t_1$) to March ($t_2$) to yield the buoyancy which is applied to the mixed-layer model. Values of the surface buoyancy vary from year to year roughly ranging from 0.5 ($m^2\ s^{-2}$) to 2.0 ($m^2\ s^{-2}$) (Fig. 12), which correspond to the buoyancy integrated for about 1.5 to 6.0 months using a typical buoyancy flux value of $1.2 \times 10^{-7}$ ($m^2\ s^{-3}$) in the LS (Marshall and Schott, 1999). The equation is numerically integrated to a depth $d$, at which the given equation holds.

The estimated MLD ($d$) is averaged over the region of deep-water formation (Fig. 6 (b)). The timeseries contains both the high frequency at the interannual timescales and the low frequency at the decadal timescales. The estimated and the obtained MLD are highly correlated ($r = 0.80$ at 0 lag) with each other with similar amplitudes (Fig. 13). This suggests that the simple one-dimensional model is capable of reproducing most of the variability in the convective activity in the LS, and that not only the surface forcing but also the oceanic internal structure seem to play the important roles in determining the depth of convection.

**Decadal timeseries**

The timeseries for both the obtained and estimated MLD from the above calculation are linearly detrended and binomial-filtered once to extract the decadal signal (Fig. 14 (a)). The correlation between the two timeseries is increased from $r = 0.80$ to 0.85. The analytical model is calculated with the yearly varying oceanic stratification in November and the climatological buoyancy, which is averaged over the period from 1952 to 1993 (Fig. 14 (b)). Both the timeseries of the obtained and estimated MLD are detrended and binomial-filtered once. They are highly correlated with each other ($r = 0.73$ at 0 lag). This suggests that the oceanic stratification at the preconditioning stage primarily dominates the MLD variabilities at the decadal timescales. In the case with the yearly varying buoyancy and the climatological oceanic stratification (Fig. 14 (c)), the modeled MLD does not correlate with the observed MLD ($r = 0.43$ at 0 lag). It seems that the role of buoyancy forcing alone does not represent the decadal processes in the region of interest. When the strength of the THC changes it

is normally related to the variations of the heat flux over the subpolar region. However, it may be possible that the variations in the THC are dominantly associated with the convection process, dependent to much less degree on the heat flux.

In order to further examine the role of each the preconditioned ocean and the buoyancy, the yearly varying oceanic stratification in November and the randomly selected buoyancy from 1952 to 1993 (Fig. 15 (a)) and the yearly varying buoyancy and the random ocean stratification (Fig. 15 (b)) are substituted into eq. 11. The random selection is done using the random data generator ($ran2$) from *numerical recipes* in such a way that an arbitrary year is picked only once out of the 42-year sample. This random run is repeated 10 times and averaged to obtain the timeseries. Except for the considerably reduced amplitudes, both the timeseries resulting from cases (a) and (b) show very similar fluctuations ($r = 0.71$ at 0 lag and $r = 0.41$ at 0 lag).

The important role of oceanic stratification in the precondition for convection seems clear for decadal timescales. The contribution of temperature and salinity to the density is shown by reconstructing the density with the yearly varying temperature and the climatological salinity in November (Fig. 16 (a)) and with the yearly varying salinity and the climatological temperature in November (Fig. 16 (b)). The virtual buoyancy is included in the calculation. This run is basically the same as Fig. 13 except that the oceanic stratification has only either the temperature or salinity component. The timeseries in the former case, i.e. Fig. 16 (a) has a similar amplitude as the directly estimated MLD and is highly correlated to it ($r = 0.86$ at 0 lag). On the other hand, the salinity

contribution to the stratification is almost zero in case of Fig. 16 (b). Thus, the oceanic thermal-driving mechanism has a great impact on the variability in the LS at these timescales.

### Local heat content change

The heat content change of the upper 500 $m$ is estimated by converting the annual cumulative surface heat flux to the potential temperature change in the water column to decouple the effect of local heat flux on the stratification in the LS. The change in the total heat content in the upper 500 $m$ is also calculated to compare with the local heat content. The upper 500 $m$ water column is considered to represent the gyre circulation and the near-surface stratification in the preconditioning is assumed to be included within the upper 500 $m$. The heat content change is a sum of advection of heat and surface heat flux. Only 15% ($SDEV2/SDEV1$) of the total heat content variance in the LS is explained by the local heat flux (Fig. 17). The difference between the two parameters is a measure of the change in strength of the gyre circulation and its ability to bring the heat anomalies from the lower latitudes. An observational study by Reverdin and Verbrugge (1999) showed that 50% of the heat content changes in the subpolar gyre can be explained by the local heat flux from 1993 through 1998, which suggests a complementary contribution from outside of the subpolar gyre.

### Remotely advected/propagated heat content

The lagged cross-correlation analysis is applied to the upper 500 $m$ heat content to examine the advected/propagated contribution of heat anomalies from

outside the LS. The studied domain in this analysis extends from $0°N$ to $70°N$ and from $100°W$ to $20°E$. The data field from the heat content is first annually averaged to form the anomalies and quadratically detrended, after which the timeseries is binomial-filtered twice to extract the decadal signals. In order to show its origin and capture the propagating features of the decadal changes in the heat content, the lagged cross-correlations are calculated between the timeseries at each point and that averaged over the region shown in Fig. 6 (b).

Positive heat content during the negative lag years indicates that the signal at 0 lag has already existed somewhere before reaching the LS. The decadal signal orginates (Fig. 18 (a)) off the east coast of the African continent, and propagates to the west as the form of decadal Rossby waves at a latitude band of $20°N$ to $30°N$ (Häkkinen, 2000) (lag -7 to -4 years). After the Rossby waves arrive at the western boundary, the enhanced signals seem to advect/propagate to the north along the western boundary (lag -4 to -2 years). The advecting/propagating features of the anomalies have been recongnized in the upper 500 $m$ heat content field, as discussed in Chapter 2, with its estimated speed of $O(2.0)\ cm\ s^{-1}$. It has been suggested that the advecting/propagating signals are the transient response associated with the changes in the THC. In particular, the northward advective/propagative anomalies were first recongnized by Sutton and Allen (1997) who analyzed the observed SST anomalies in this region. Because of their slow moving speed ($\sim 1.7\ cm\ s^{-1}$) they speculated that the SST signals represent the upper ocean transport below the mixed-layer. Other observational data reveal the decadal signals in the subsurface in the western boundary current (Molinari et al., 1997). The observational evidence supports

the advective nature of the upper heat content along the Gulf Stream.

During the lag of -2 to 0 years, the positive heat content from the Gulf Stream rapidly spreads to the region of deep-water formation in the LS. The evolution of the heat content anomalies suggests that those over the Gulf Stream are related to the gyre-scale changes imparted by Rossby waves in this latitude band, and that the anomalies propagate to the subpolar gyre. The decadal variations in the LS seem to be controlled by the lower latitude water via the change in heat content.

### 3.5 Summary and conclusion

A 43-year subset of output from a coupled ice-ocean model has been analyzed to study the decadal variability in the Labrador Sea (LS). The high surface densities or the deepest mixed-layer in March, indicating the convective region, are located along the continental slope, off the eastern Labrador coast. The surface density field has the largest values in March 1973, 1983 and 1993, indicative of decadal oscillations. Evidence of the decadal variability in the convective activity is also seen in the temperature versus time diagram. Every year the mixing reaches a depth of at least 1000m. Among those are distinctively strong events that occur from 1971 to 1972 and from 1983 to 1984 , reaching the depths greater than 2500 $m$. The modeled data reproduce the frequency of the convective events that are seen in the observations (Curry and McCartney, 1996) relatively well at the decadal timescales.

The cyclonic circulation in the LS sets up a favorable condition for deep convection, where the domed ispycnals play a role of oceanic preconditioning. The precondition in November significantly contributes to not only the deter-

mination of the convective site but also the convective depth. Sharply domed isopycnals near the surface increase the vertical density gradient there. The stronger the near-surface stratification at the preconditiong stage, the deeper the convective mixing.

A one-dimensional simple mixed-layer model is used to diagnose the mixed layer depth (MLD) in March from the oceanic density profile in November and the external buoyancy forcing, and compare with the MLD directly obtained from the output of the coupled ice-ocean model in March. The simple model reproduces most of the variability in the convective depth in the LS at the decadal timescales ($r = 0.85$ at 0 lag). With a yearly varying oceanic density profile in November and the climatological buoyancy the model produces the decadal fluctuation considerably well ($r = 0.73$ at 0 lag). The oceanic stratification at the preconditioning stage primarily dominates the MLD variabilities. It seems that the surface buoyancy does not predominantly participate in the decadal processes in the region of interest. With radomly selected forcing the timeseries derived from the simple model show the similar variability as above with considerably reduced ampltudes. Furthermore, the oceanic density profile, calculated from the yearly changing temperature and the climatological salinity, reproduces the variability very similar to that of the model density, suggesting that the variability of the vertical stratification is associated with temperature changes in the upper ocean. This leads to the conclusion that decadal variability in the LS may be attributed to the change in the upper ocean heat content.

A direct impact of the ice melt/freshwater on the intensity of the convection is not found in this study. The results rather show the importance of the

thermal forcing without involving salinity variability. The correspondence between the temperature and the salinity was pointed out by numerous studies, one of which was by Belkin et al. (1996). The timeseries of the model SSTA is highly correlated to the observation (Fig. 9) especially after 1960 ($r = 0.84$ at 0 lag), on the other hand, that of the model SSSA does not resemble the observational salinity variations (Fig. 10) in amplitude and phase. The variance of the summer salinity in the model is roughly 15 times smaller than that of Houghton. Häkkinen (2000) argued that sea ice is likely to participate merely to enhance and modify the cycle, passively responding to the existing decadal cycle. In fact, periods of the low salinity anomalies shown by Reverdin et al. (1997) coincide with those of weak convection due to anomalously weak heat loss.

It is plausible that the convective activity shows the decadal oscillations even with the lack of proper parameterization in the salinity, and there leaves the possibility that the LS variability is associated with the basin-wide oscillations via the upper ocean temperature variations. In Chapter 2, the variability of the basin-wide decadal oscillations in the North Atlantic has been discussed. The upper 500 $m$ heat content field showed clear quasi-decadal variations, in which anomalous signals emanated from the eastern boundary in the mid-latitudes and propagated to the west. After arriving at the western boundary the signals travelled northward until they reached the subpolar region where the deep-water formation is located. The advecting/propagating features of the anomalies coincide with those from the analysis in this study (Fig. 18), both in the timing and the spatial pattern. Further analysis, using the vertically integrated

stream function and the index to represent the THC, showed the dynamical link between the horizontal and meridional circulation through the *JEBAR*. Responding to the THC changes the entire North Atlantic seems to adjust to a new phase in the decadal cycle by the Rossby adjustment, which furthermore changes the THC through the convection process. Häkkinen (2000) suggested a potential air-sea coupled mode to generate and maintain the decadal oscillations in the whole North Atlantic domain. The basin-wide oscillations are attributed to the THC or MOC changes that are a result of variations in the volume in the LSW. She hypothesized that there exists a positive feedback between the subpolar heat fluxes and upper ocean temperatures, and a negative feedback of the MOC works on itself. The air-sea interaction between the positive and negative feedback creates the oscillatory nature by changing the strength of the MOC. However, what the results from Fig. 14, Fig. 17 and Fig. 18 in this study imply is that to the first order the decadal oscillation in the THC is closed within the oceanic circulation. The variability in the convection largely depends on the state of the oceanic stratification. Of course, the byoyancy flux or heat flux in the subpolar somehow works to reinforce and maintain the oscillation. Stronger convection forms a thicker layer of LSW compared to a weaker event. The changes in the convective depth induce the oscillations in the pressure field by forming the water masses to various depths in the LS, even fixing the buoyancy flux as climatological. In this scenario, there is a strong possibility that the decadal signals are imparted through wave dynamics in the forms of Kelvin and Rossby waves, the latter actively participated in the discussion of the basin-wide oscillations.

The present study focuses on the decadal variability of the convection in the LS and it turns out that the convection is tightly linked to the basin-scale oscillations that involve the variations of the THC. Both the basin and regional oscillations are primarily driven by the upper ocean temperature variations associated with the changes in the oceanic stratification.

# 4. Summary and Concluding Remarks

A prognostic coupled ice-ocean model has been used to investigate the 12-14 year variability that exists in the anomalous fields of the model output. An advantage of using this model is that it simulates both the Arctic and the Atlantic Ocean with the realistic forcing fields which implicitly contain the coupled mode.

It became clear that the THC is a central component in inducing the 12-14 year oscillations at the basin-scale. Associated with the changes in the THC the horizontal circulation adjusts to a new oceanic state. During this transition, it seems that Rossby waves appear from the eastern boundary in the mid-latitude and propagate to the west, and then the anomalies are advected to the sub-polar region. We have shown that these signals exist in the upper 500 $m$ heat content and the vertically integrated volume transport. Seager et al. (2000) carried out air-sea coupled numerical experiments, which were forced with the observational wind field, and came to a conclusion that the variability in the SST anomaly longer than interannual timescales (i.e. decadal timescales) is explained as a response to changes caused by the atmospheric circulations. They further concluded that the oceanic heat transport does not play a significant role in the decadal oscillations. However, as clearly demonstrated in the present study, the anomalies in the upper heat transport play a major role in determining the convective activity that is strongly associated with the THC variations. The variations in the convection may possibly be induced with the upper ocean

temperature variations even by prescribing the buoyancy flux, or heat flux, as climatological. Besides, Visbeck et al. (1998) suggested from their numerical experiments that the SST anomalies are tightly linked to the atmospheric circulations whereas the upper ocean anomalies have little contribution. Their work still supports our result that the upper ocean transport plays a significant role in the decadal mechanism. It is an open question yet to be answered by future study whether the changes in the ocean heat transport leads or lags the development of the SST anomalies. This may answer the question of whether the ocean or atmosphere dominates the decadal oscillations.

The question addressed in the introduction of whether the decadal oscillations are derived and maintained from the system that involves the air-sea coupled or ocean-only mode has not been made clear from this study. The existence of air-sea coupling was suggested by Häkkinen (2000) in the western boundary and subpolar regions. She hypothized that the basin-wide oscillations are attributed to the THC or MOC changes that are a result of variations in the volume in the Labrador Sea Water (LSW), and that there exists a positive feedback between the subpolar heat flux and upper ocean temperatures and a negative feedback of the MOC works on itself. The air-sea interaction between the positive and negative feedback induces an oscillatory behavior by changing the strength of the MOC. To the first order, however, the oscillations seem to be induced by the variations in the ocean-only system that prominantly involves the THC. We conclude that the THC variations are associated with the variations of the convective activity controlling the LSW depths and induces the oscillations in the pressure field in the LS. Remember that the convective ac-

tivity is strongly controlled by the oceanic stratification, which is influenced by the subtropics. This leads to a possiblity that the decadal oscillations actively involve the wave dynamics in the ocean-only mode with the help of advection (schematic figure for this mechanism is shown in Fig. 19). The disturbances created by the pressure changes could propagate as the form of Kelvin waves along the western boundary southward, along the equator eastward and along the eastern boundary northward. The Kelvin waves that arrive at the eastern boundary excite the Rossby waves to radiate from this region to the interior ocean and eventually they reach the western boundary, similar to the Rossby propagation repeatedly discussed in the previous chapters. In this sense, the Rossby waves play a role to relay the signals back to the THC region, perhaps in order to maintain and close the decadal cycle. A dynamical explanation of exactly how the Rossby and Kelvin waves are generated should be shown in future studies. For this purpose, it is necessary to find evidence of the Kelvin wave propagation, which did not obviously appear in our model due to the limited frequency of model output (only monthly values obtained from the model).

The above scenario points to the convection process as a central mechanism of the decadal oscillations. Our initial attempt to discuss the impact of ice on the THC variations seems to be discarded in this study. However, it is still an important issue to quantify how much impact the ice component gives on the system in the decadal regime, in the light of the THC variations, as predicted by Mauritzen and Häkkinen (1997). Analysis of the observational data in and near the LS may also elucidate the dynamics regarding this issue, in spite of the lack of spatial and temporal coverage.

## 5. Acknowledgments

I would like to thank the committee members, Drs. James J. O'Brien, Sirpa Häkkinen, Steven D. Meyers, Eutiquio Young, Richard L. Iverson, Doron Nof and Georges Weatherly for their time and helpful comments regarding the contents of this study. Special thanks to my major professor Dr. James J. O'Brien for his patience and support for allowing me to work at COAPS, and especially for encouraging me to do independent research.

I would also like to thank Dr. Nobuo Suginohara for his useful discussions and scientific in-depth advice.

The output from numerical simulations examined in this study were conducted at the Goddard Space Flight Center, by Dr. Sirpa Häkkinen.

I would like to express my gratitude to my fellows at FSU (Steven Morey, Francisco Sandoval, Luis Zamudio, A. Birol Kara, Thierry Penduff and Jorge Zavala) for their academic support during the Ph.D. program.

# 6. Figures

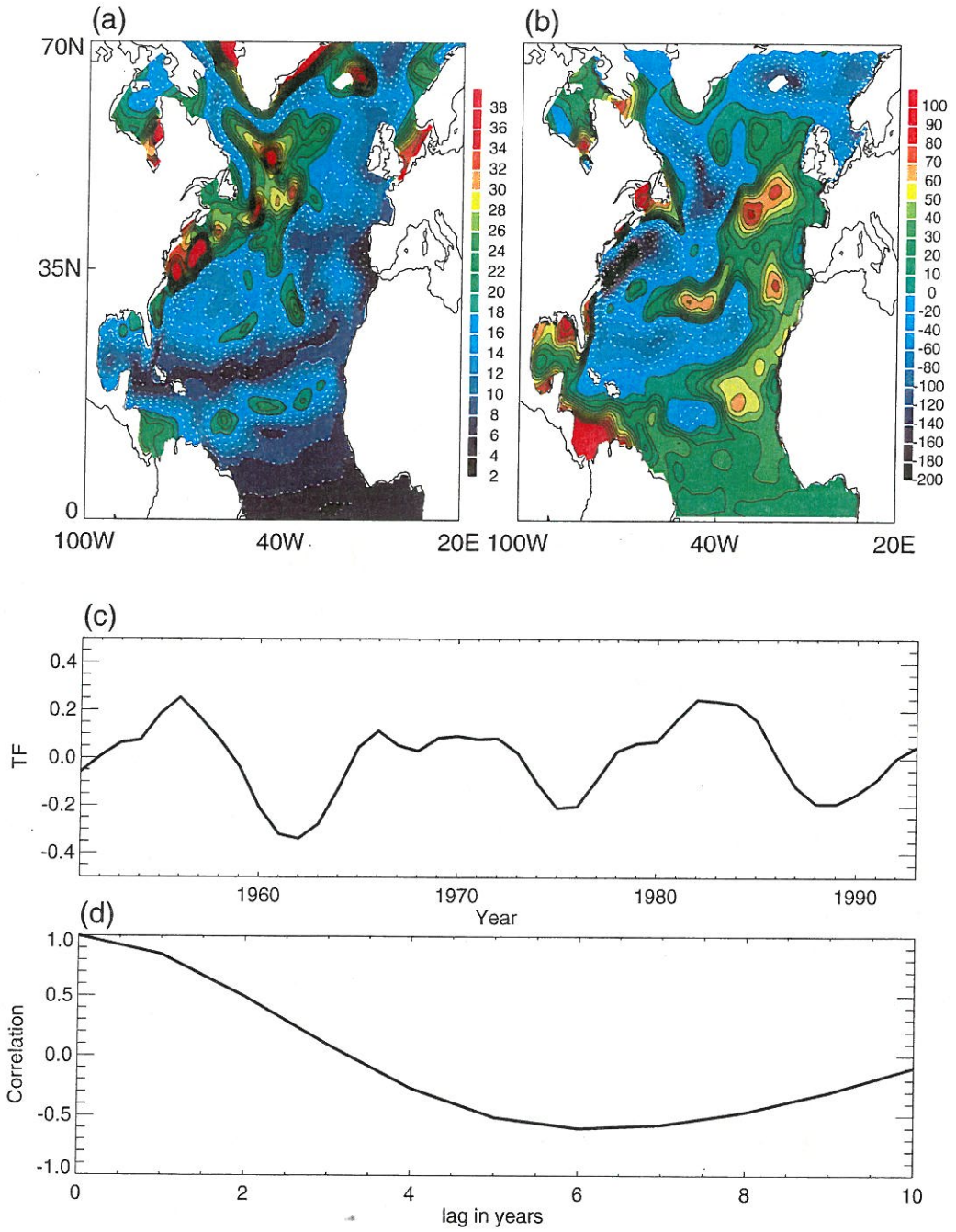


Figure 1: (a) Standard deviation ($°C$) from the mean over the period from 1951 to 1993 for the upper 500 $m$ heat content. The values are multiplied by 100. The contour interval is 2. (b) spatial function of the EOF mode 1. The values are multiplied by 100. The contour interval is 10 for the positive values and 20 for the negative values. (c) temporal function of the EOF mode 1 (d) autocorrelation of the EOF mode 1. The largest negative correlation is roughly at 6 year lag.

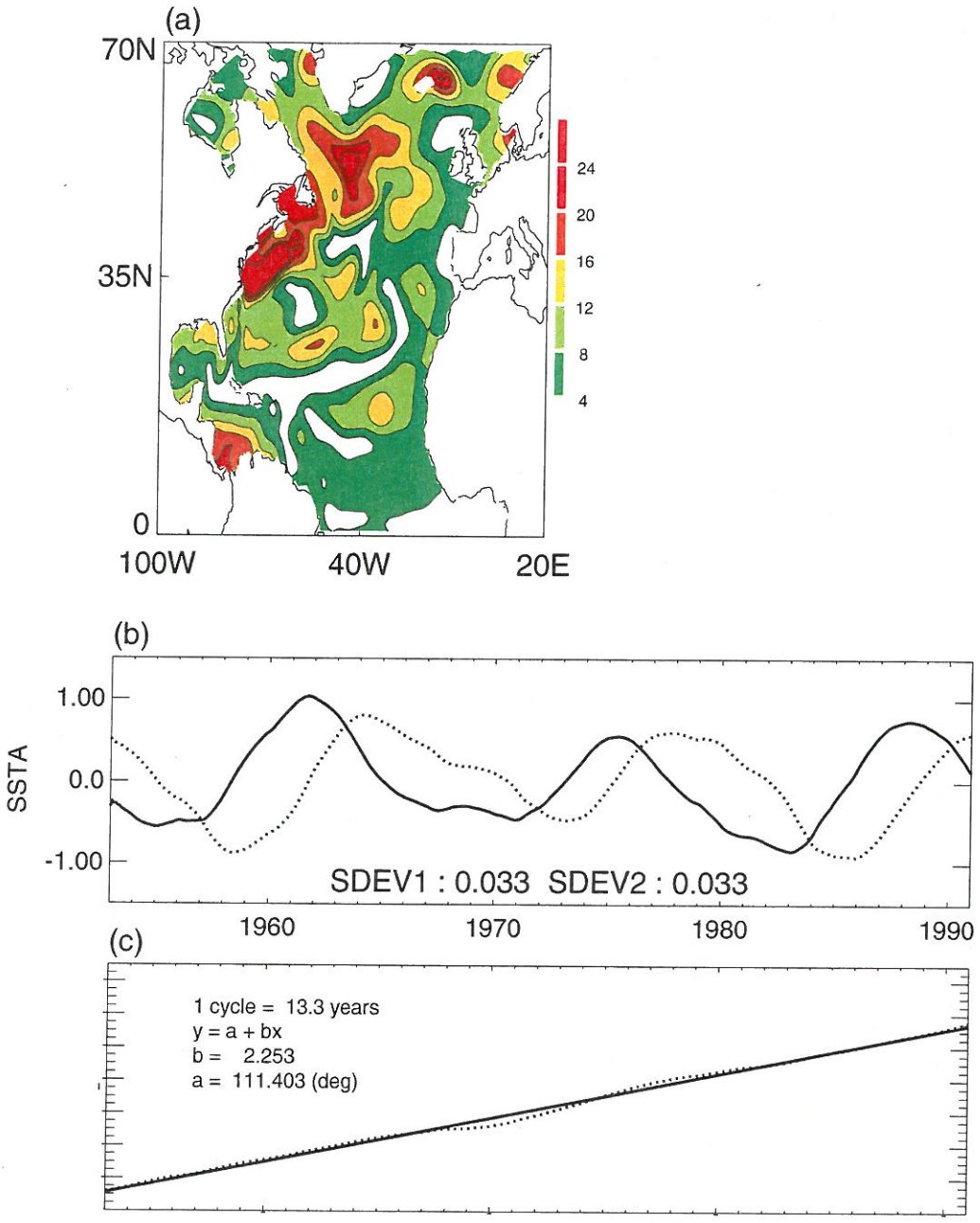


Figure 2: (a) Spatial amplitude function obtained from the CEOF mode 1 multiplied by 100. (b) Temporal functions obtaind from CEOF mode 1. The solid line represents the timeseries of the real part and the dotted line is the imaginary part. $SDEV1$ and $SDEV2$ are respective standard deviations for the real and the imaginary parts. (c) The dotted line is the temporal phase function obtained from the CEOF mode1. The solid line is the best fit to the functions.

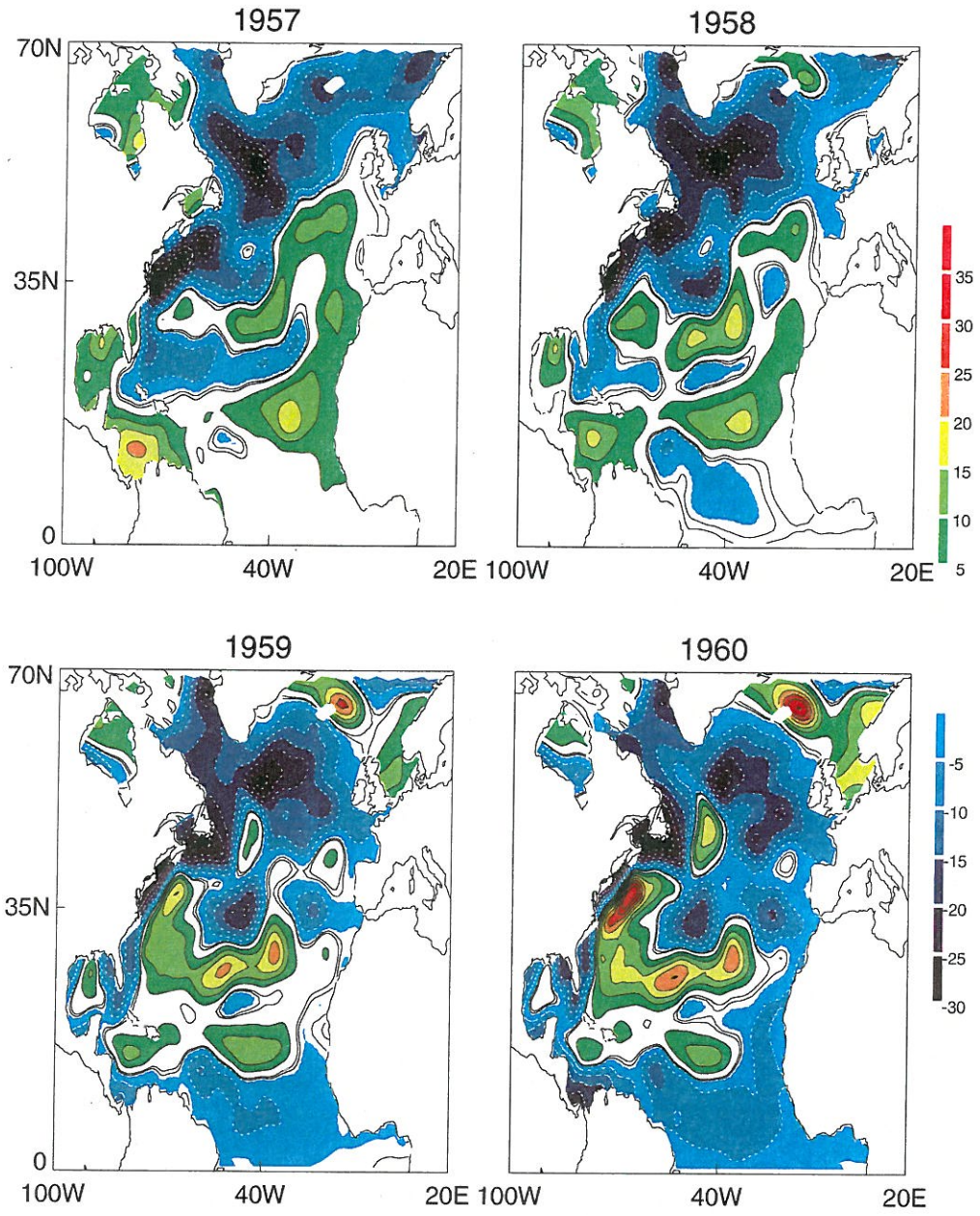


Figure 3: Sequence from 1957 through 1964 of the annually averaged reconstructed upper heat content anomalies obtained from the CEOF mode 1 (4-year low-pass filtered). The values are multiplied by 100. Units are in degrees Celsius.

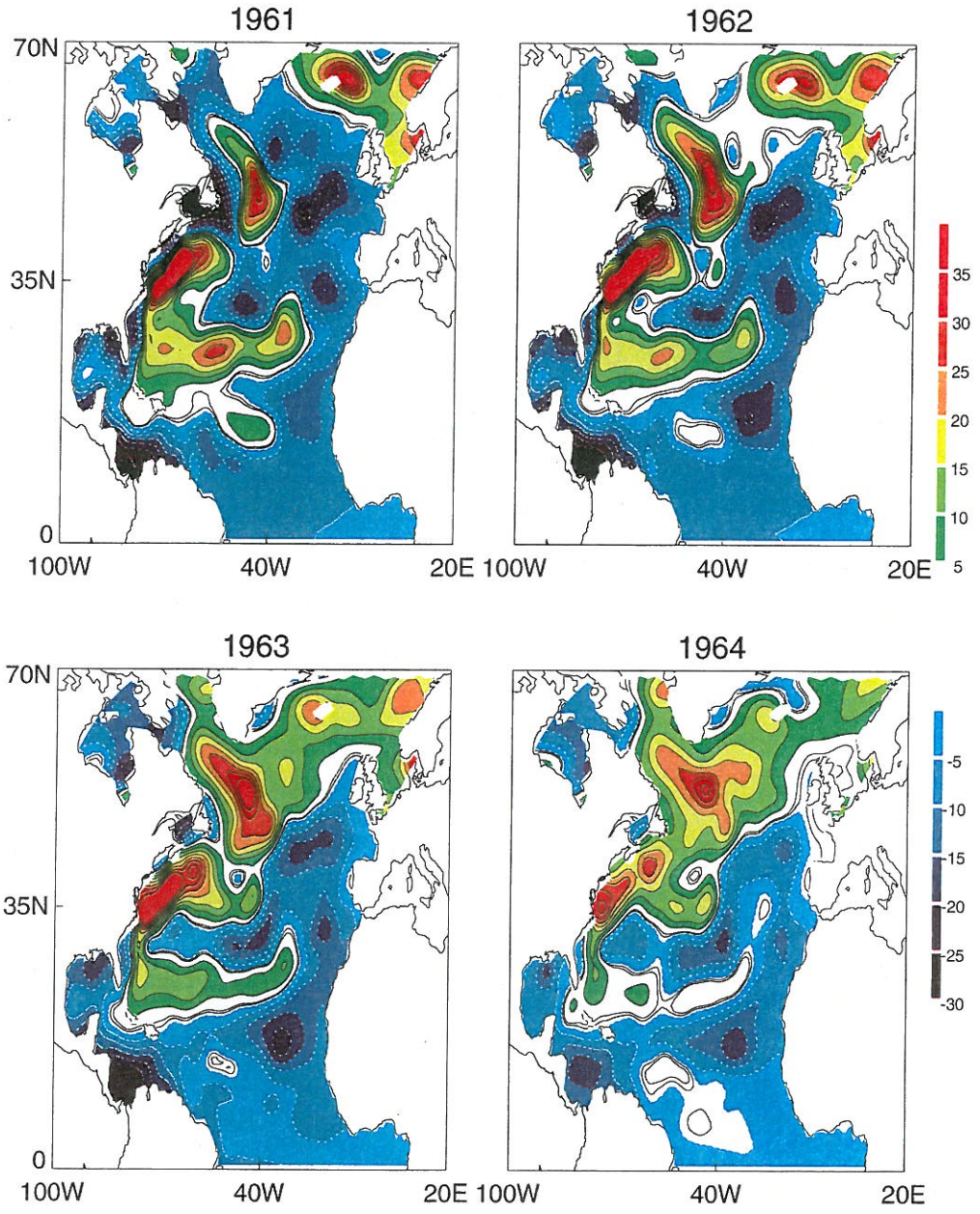


Figure. 3 (cont)

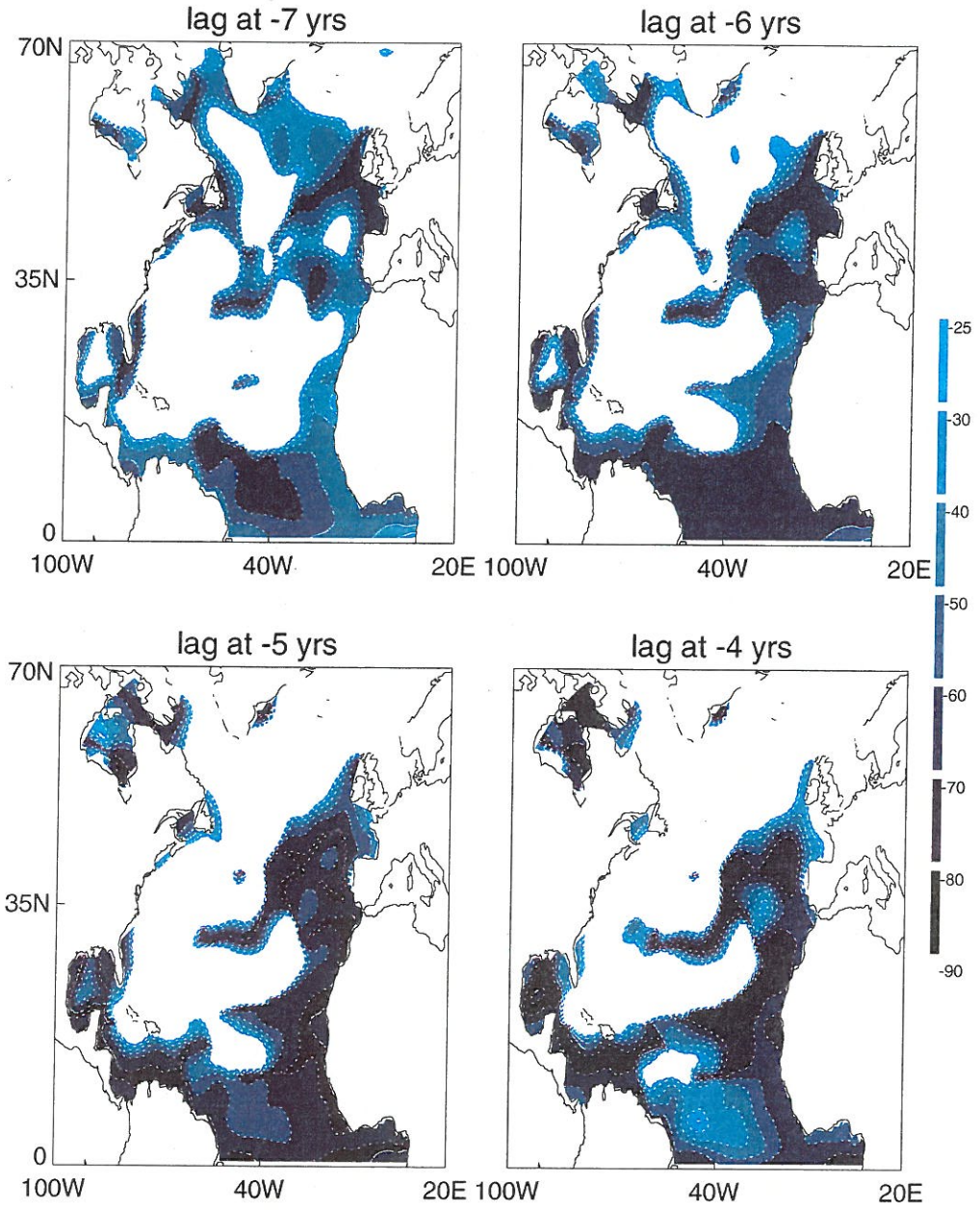


Figure 4: The cross-correlation of the CEOF mode 1 from the upper 500 $m$ heat content and EOF mode 1 from the stream function, both of which are the same as those discussed above. The correlations are multiplied by 100 and above 30 are significant at 95 % level. The correlation are shown at the lag from -7 to 0 years before the extrema in EOF 1 in the stream function.

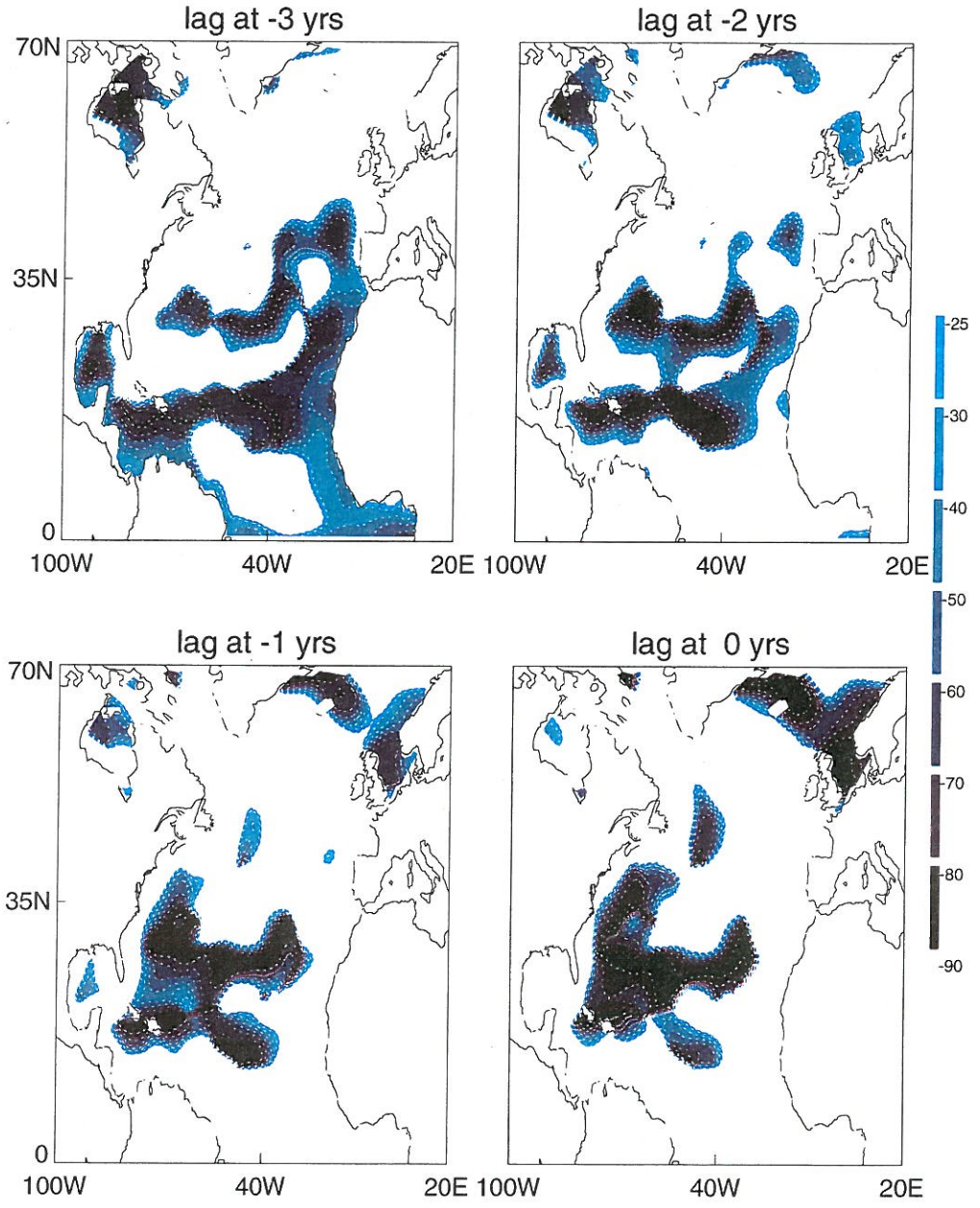


Figure. 4 (cont)

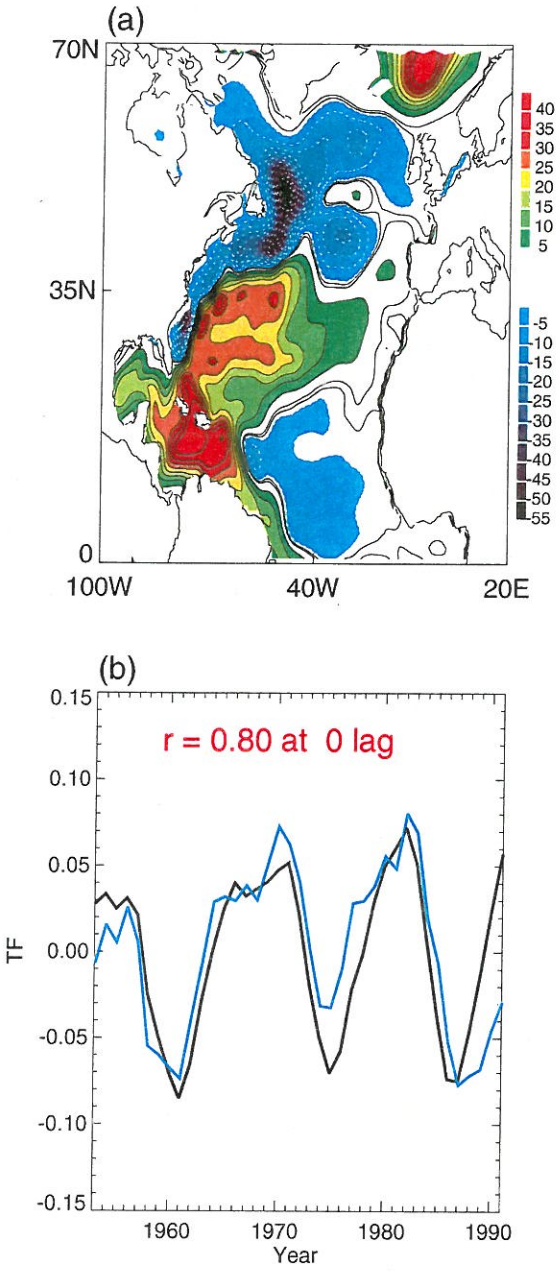


Figure 5: (a) Spatial function of the EOF mode 1 for the vertically integrated stream function. The values are multiplied by 100. The contour interval is 10 for the positive values and 20 for the negative values. (b) Temporal function of the EOF mode 1 (black line) from 1953 through 1991. The blue line is the timeseries from the MHT at $30°N$. Both the timeseries are highly correlated with each other ($r = 0.80$ at 0 lag).

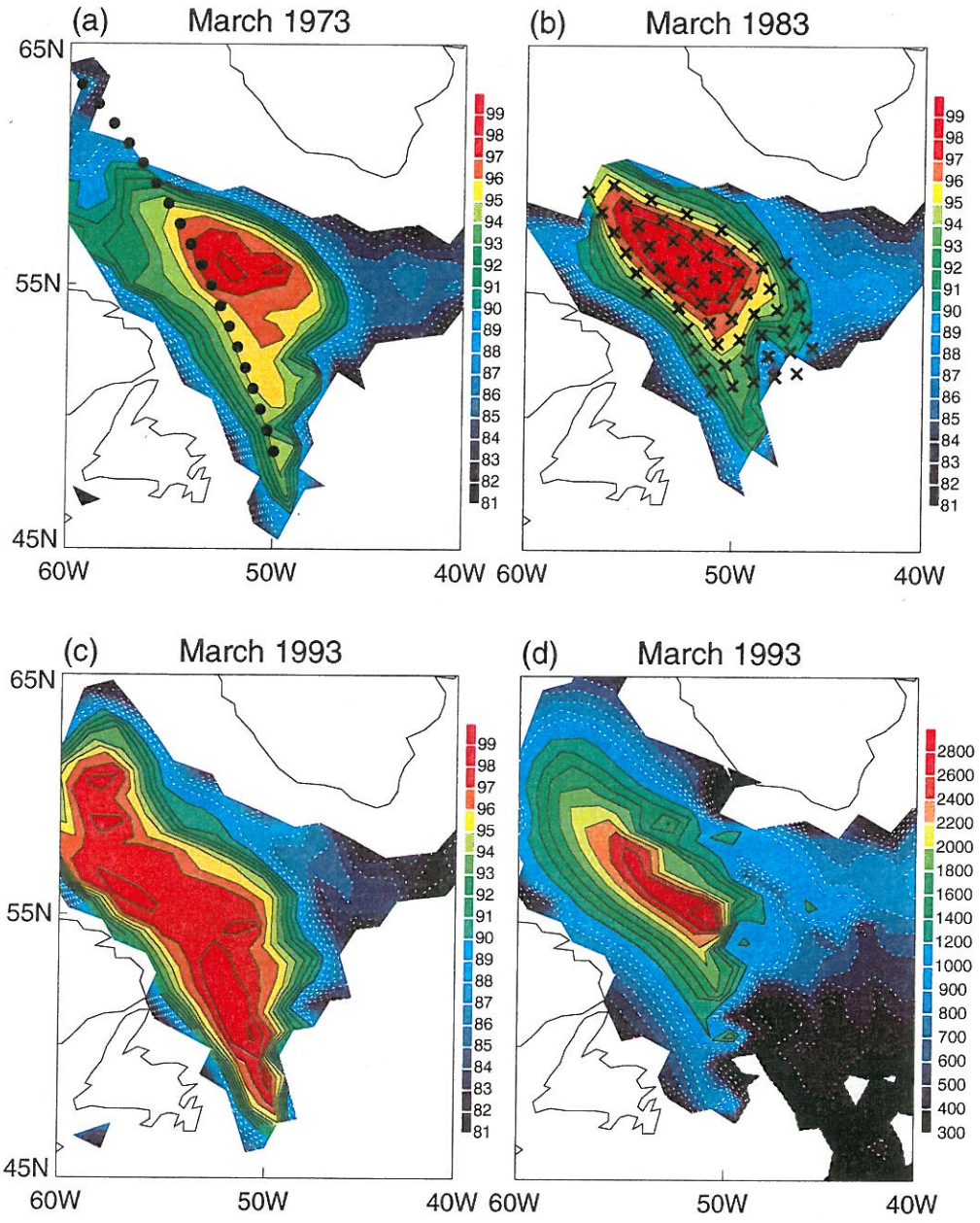


Figure 6: Potential density ($(\sigma_\theta - 27.00)$ $(kg/m^3)$ $\times 100)$) fields at the surface in March (a) 1973 (b) 1983 (c) 1993. Only the values above 80 are contoured to highlight the region of deep-water formation. (d) mixed layer depth (MLD) in March 1983. The MLD is defined as the depth at which the vertical density difference is less than or equal to 0.005 $(kg/m^3)$. The MLD greater than 200m is contoured. The vertical cross-sections are chosen along the black circles. The crossed-region is considered as the center of convective action and it is averaged to obtain the timeseries.

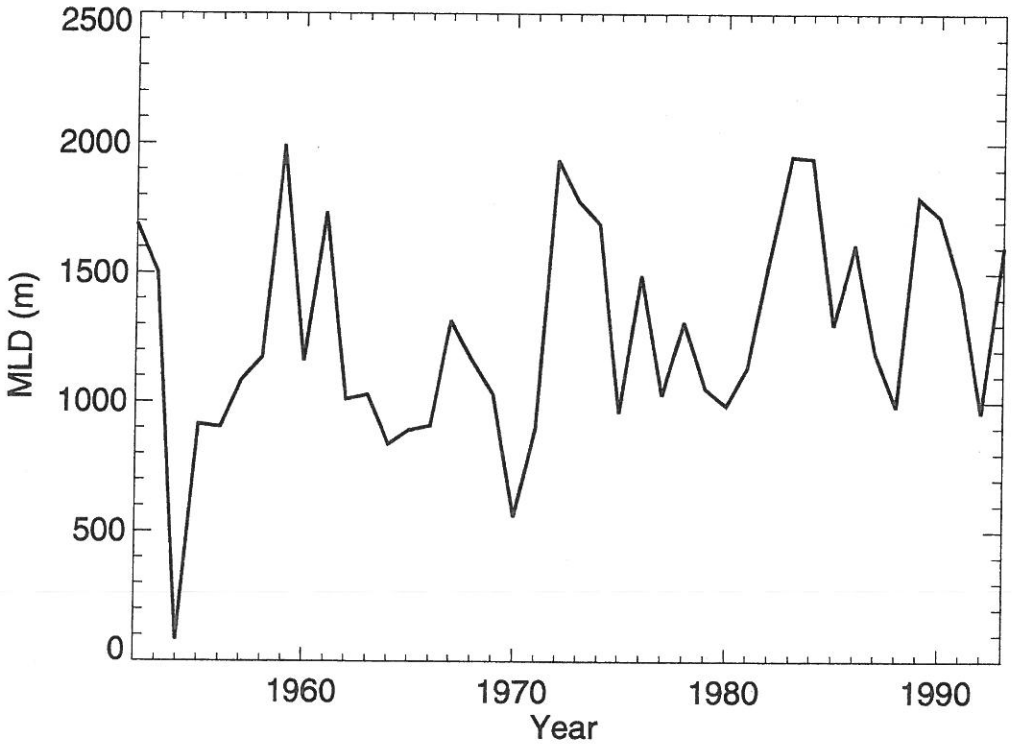


Figure 7: Timeseries of the MLD in March from the model output. The timeseries is averaged over the region shown in Fig. 6 (b).

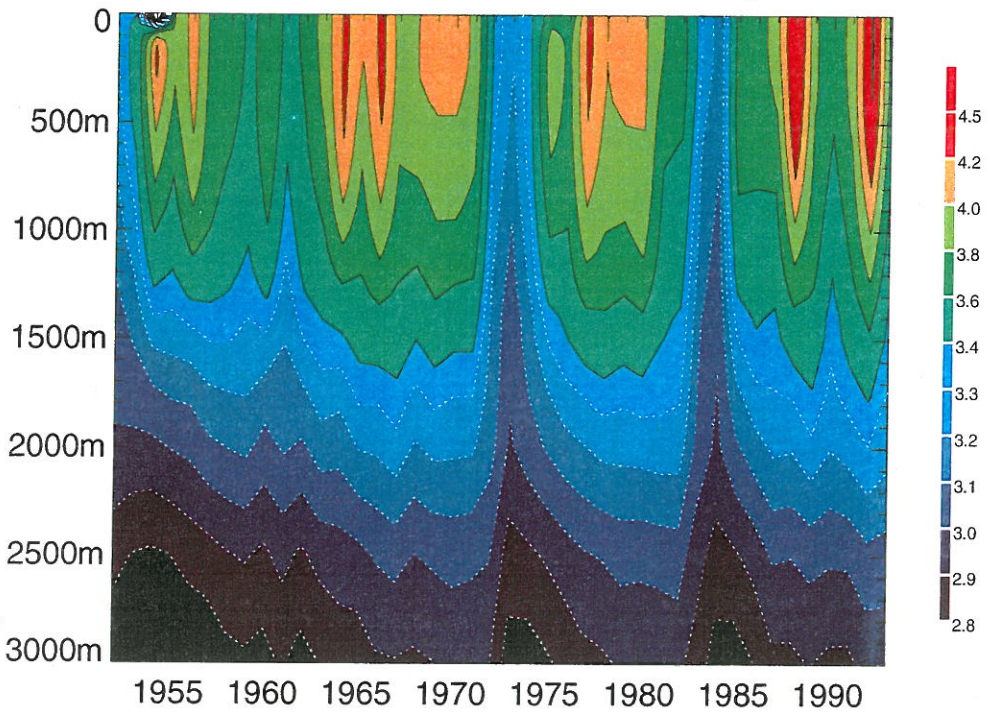


Figure 8: Depth vs. time diagram of the potential temperature in March from 1951 through 1993 averaged over the region shown in Fig. 6 (b). The temperature varies from 1.9° $C$ to 4.4° $C$.

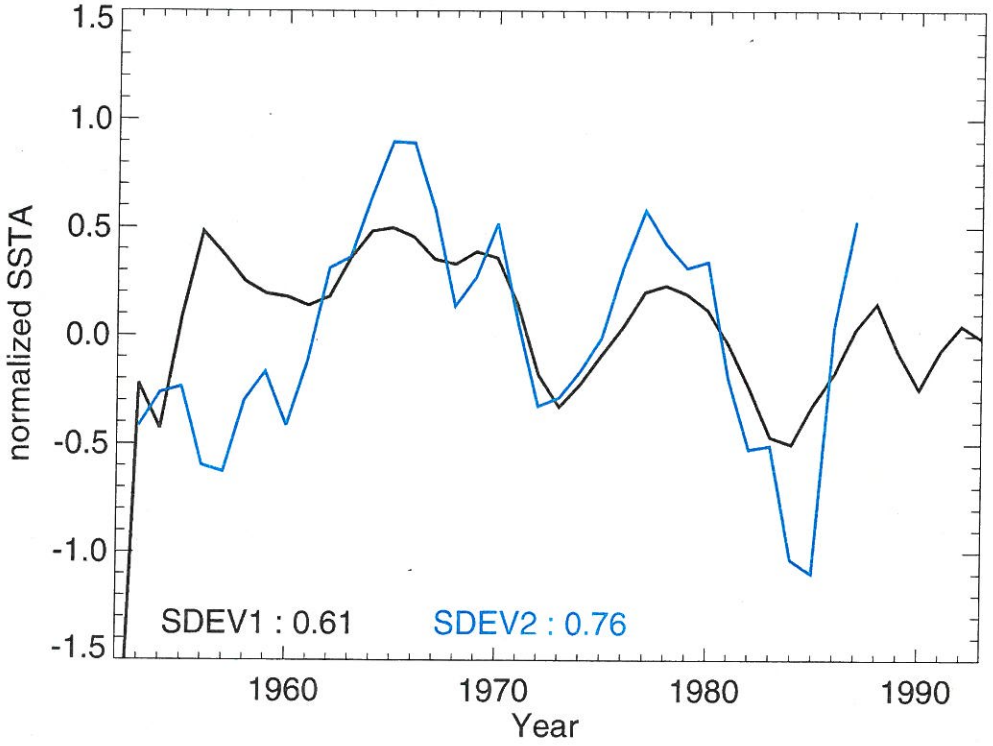


Figure 9: Sea surface temperature anomalies (SSTA) in March binomial-filtered once, linearly detrended and normalized by twice their respective standard deviation ($SDEV1$, $SDEV2$). The black line is the SSTA in March obtained from the coupled ice-ocean model, averaged over the region shown in Fig. 6 (b). The blue line is the SSTA timeseries from 1953 through 1987 from Houghton (1996) in March. Both timeseries from 1960 to 1987 are highly correlated with each other ($r = 0.84$ at 0 lag).

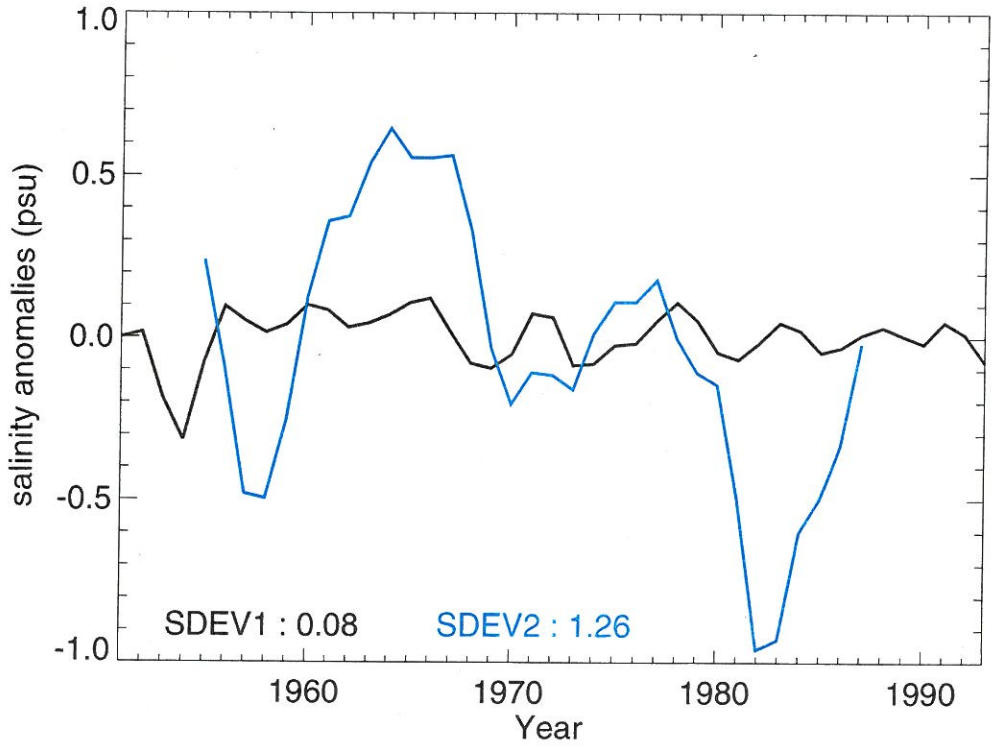


Figure 10: Sea surface salinity anomalies (SSSA) in August (summer). The black line is the SSSA in August obtained from the coupled ice-ocean model, averaged over the region shown in Fig. 6 (b). The blue line is the SSSA time-series in summer from 1955 through 1987 from Houghton (1996). Both time-series are linearly detrended and binomial-filtered once. Note that they are not normalized.

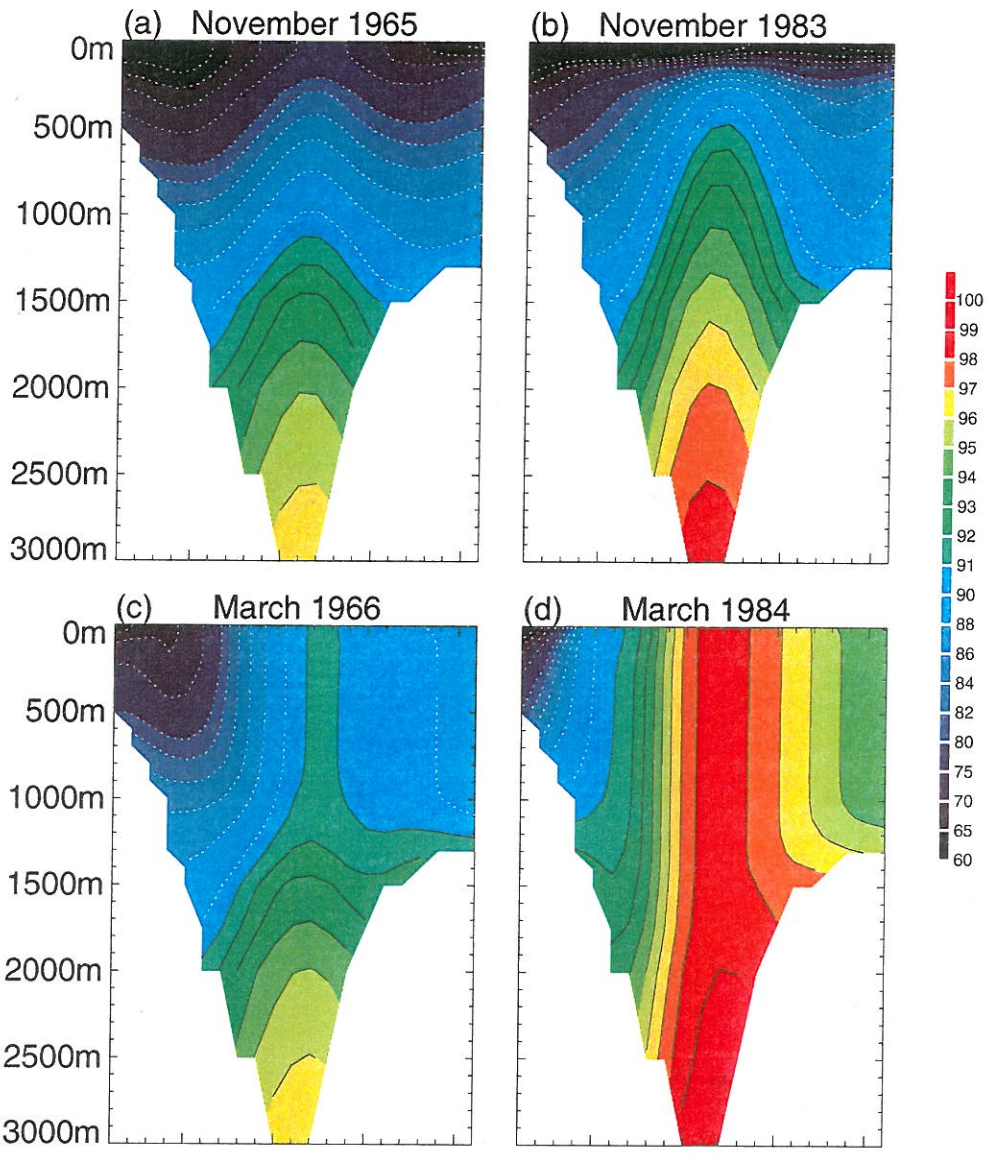


Figure 11: Vertical cross-sections along the line (black circles) shown in Fig. 6 (a). They are viewed from the Newfoundland. (a) precondition in November 1965 (b) precondition in November 1983 (c) violent mixing in March 1966 (d) violent mixing in March 1984. The values are $(\sigma_\theta - 27.00)$ $(kg/m^3)$ $\times 100$, of which only the values above 80 are contoured to highlight the region of deep-water formation. Hanning-filtering three times in space is applied to make the field smooth.

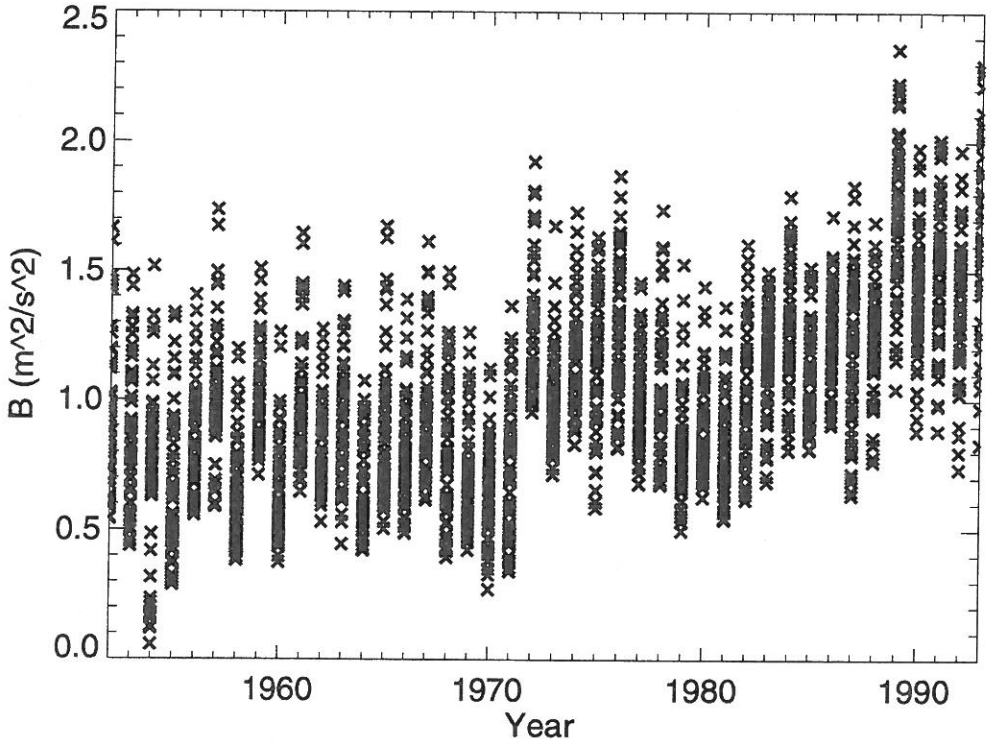


Figure 12: Buoyancy ($m^2\ s^{-2}$) estimated by integrating the buoyancy flux from November to March in each year over the region of deep-water formation shown in Fig. 6 (b). All the values over this region are plotted. The buoyancy flux is estimated from the heat and salinity flux obtained from the coupled ice-ocean model.

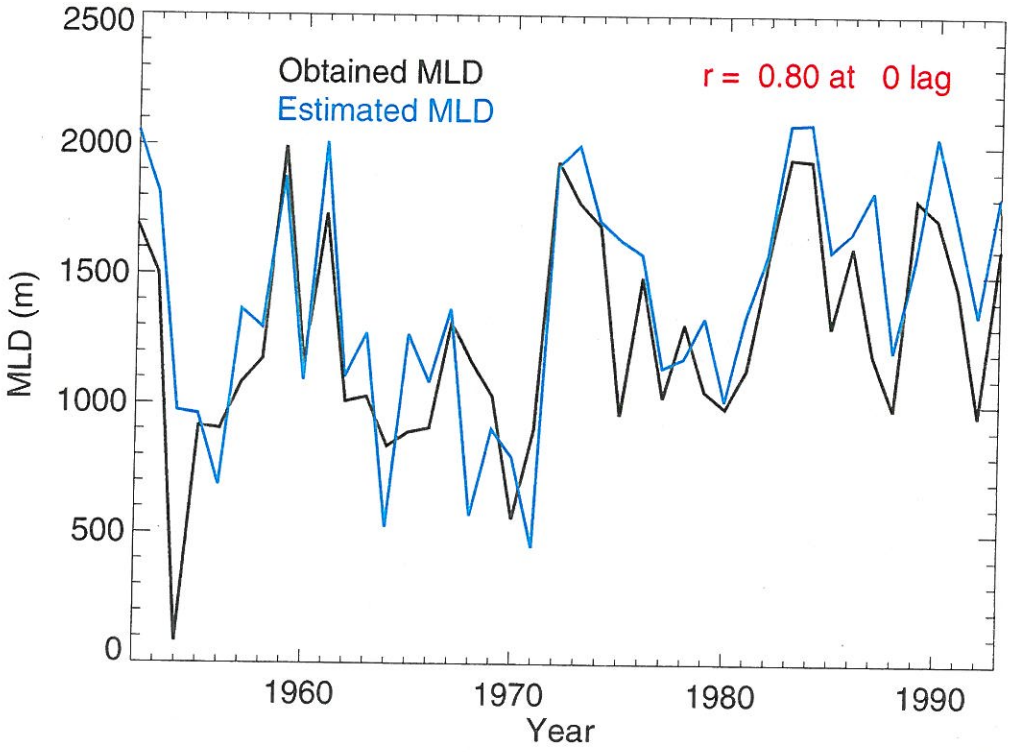


Figure 13: Timeseries of obtained MLD (black line) in March from the model output and estimated MLD (blue line) in March diagnosed using a simple one-dimensional analytical model (eq. 11). Both the timeseries are averaged over the region shown in Fig. 6 (b).They are highly correlated with each other with the cross-correlation coefficient of $r = 0.80$ at 0 lag.

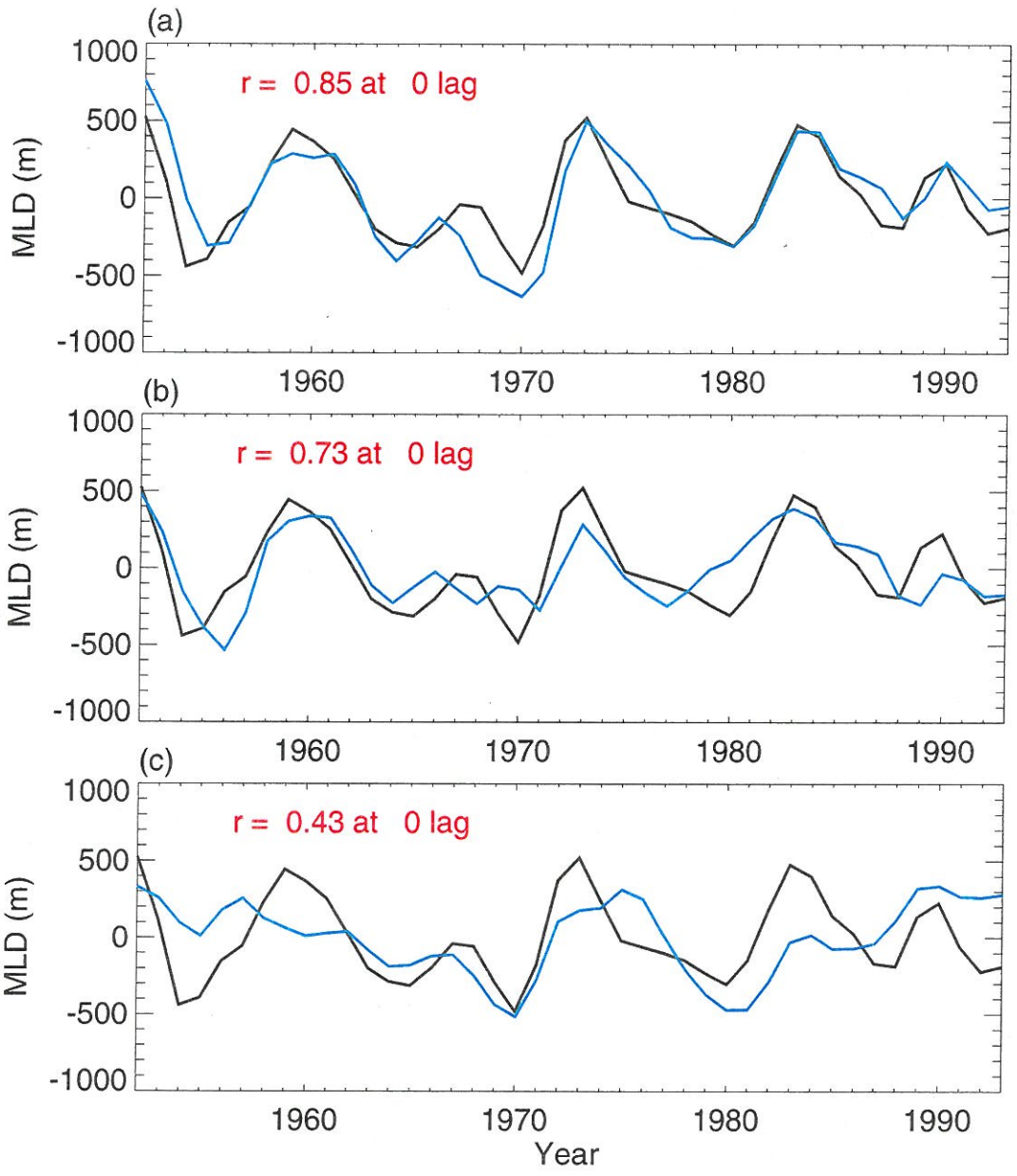


Figure 14: (a) Same as Fig. 13. Same as Fig. 13 except that (b) Timeseries of the estimated MLD (blue line) obtained from the simple model forced with realistic ocean stratification in November and the climatological buoyancy. (c) with climatological ocean and realistic buoyancy. All of the timeseries are linearly detrended and binomial-filtered once. The cross-correlation coefficients at 0 lag (red) between the two timeseries are shown on the upper left corner.

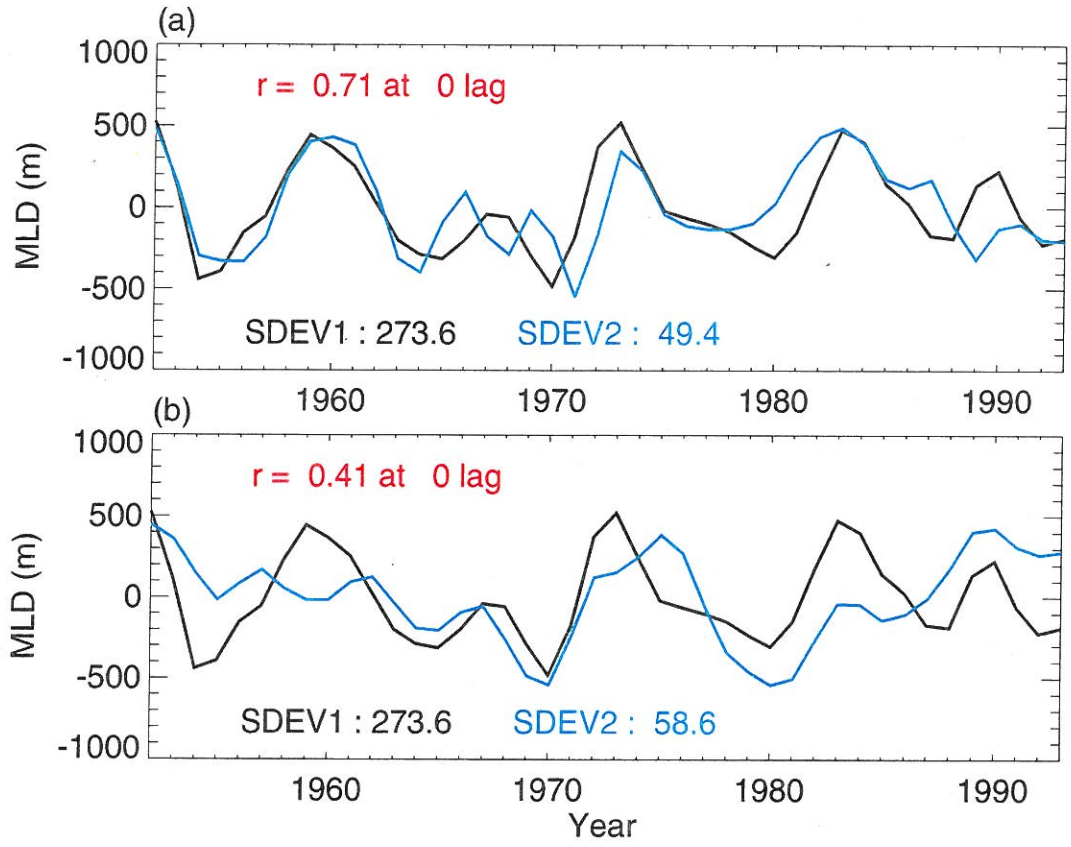


Figure 15: Same as Fig. 14 except that (a) the timeseries of estimated MLD (blue line) is forced with the realistic ocean stratification in November and randomly selected buoyancy and (b) with realistic buoyancy and randomly selected ocean stratification in November. $SDEV1$ (black) is the standard deviation of the observed MLD and $SDEV2$ (blue) the estimated MLD. Note that the timeseries of estimated MLD is multiplied by $(SDEV1/SDEV2)$ to make the amplitudes of the two timeseries comparable.

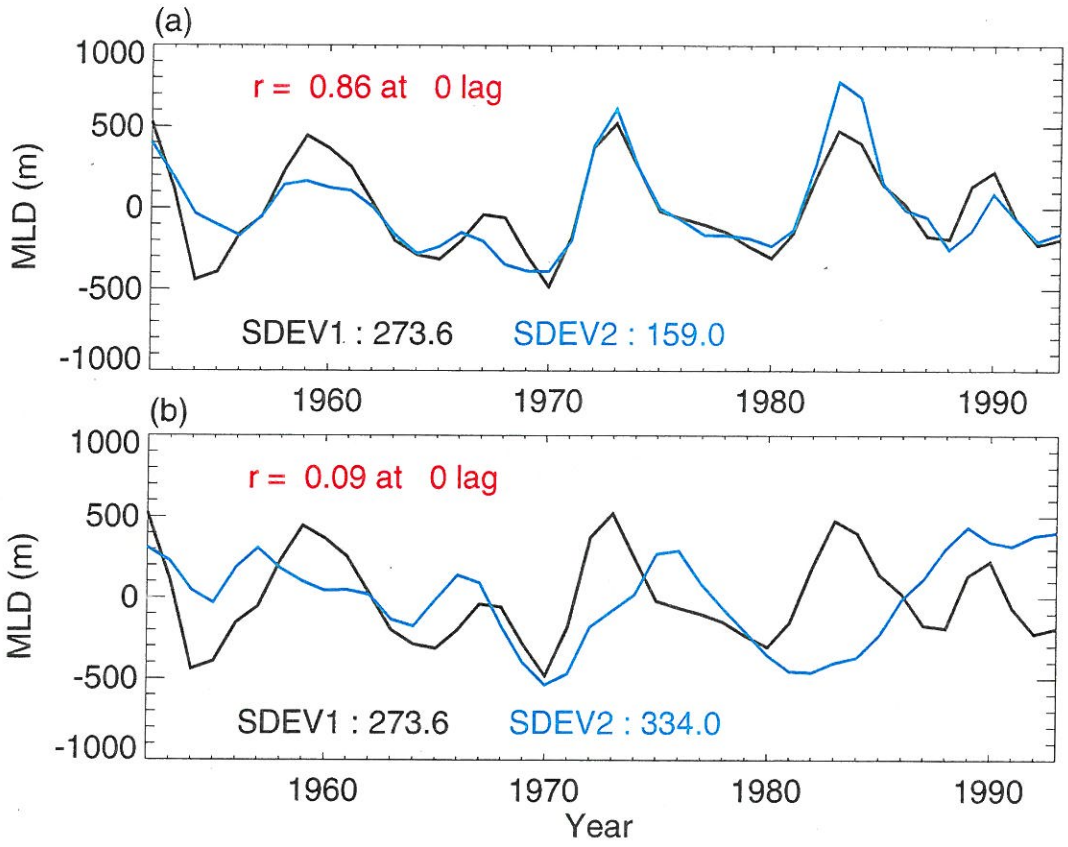


Figure 16: Same as Fig. 13 except that (a) the timeseries of estimated MLD (blue line) whose oceanic stratification in November is constructed with the realistic temperature and the climatological salinity. (b) with realistic salinity and the climatological temperature. $SDEV1$ (black) is the standard deviation of the observed MLD and $SDEV2$ (blue) the estimated MLD. Note that the timeseries of estimated MLD is multiplied by $(SDEV1/SDEV2)$ to make the amplitudes of the two timeseries comparable.

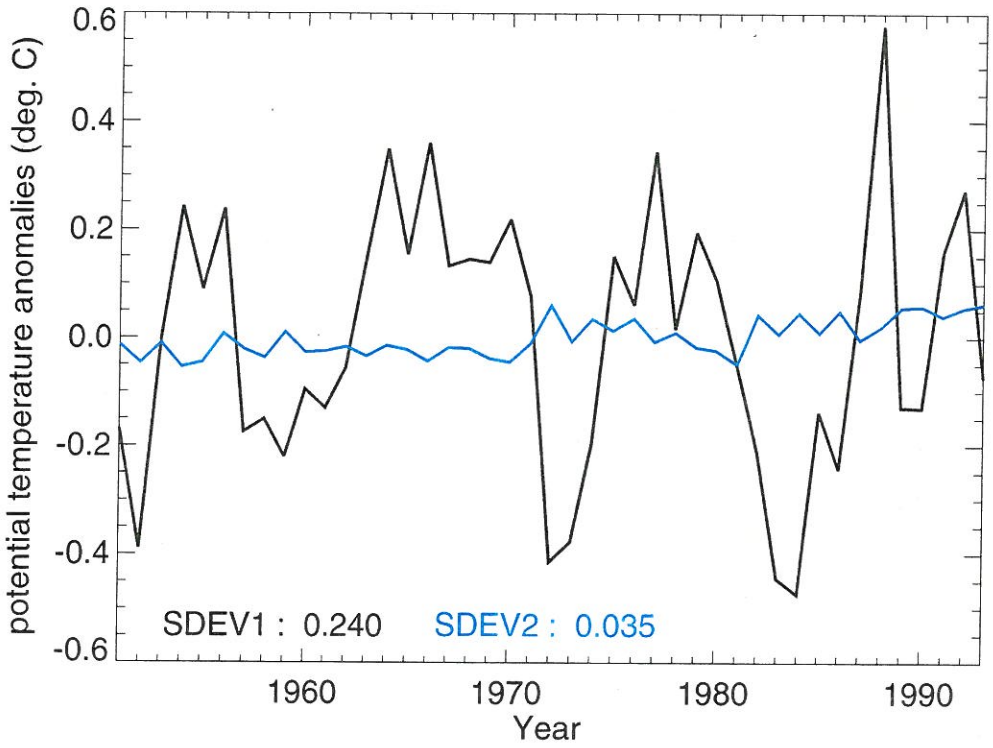


Figure 17: The change in heat content of the upper 500m from year to year (black line) and the annual cumulative surface heat flux (blue line) converted to a potential temperature change in the same 500m water column. SDEV1 (black) is the standard deviation of the heat content and SDEV2 (blue) the converted heat flux.

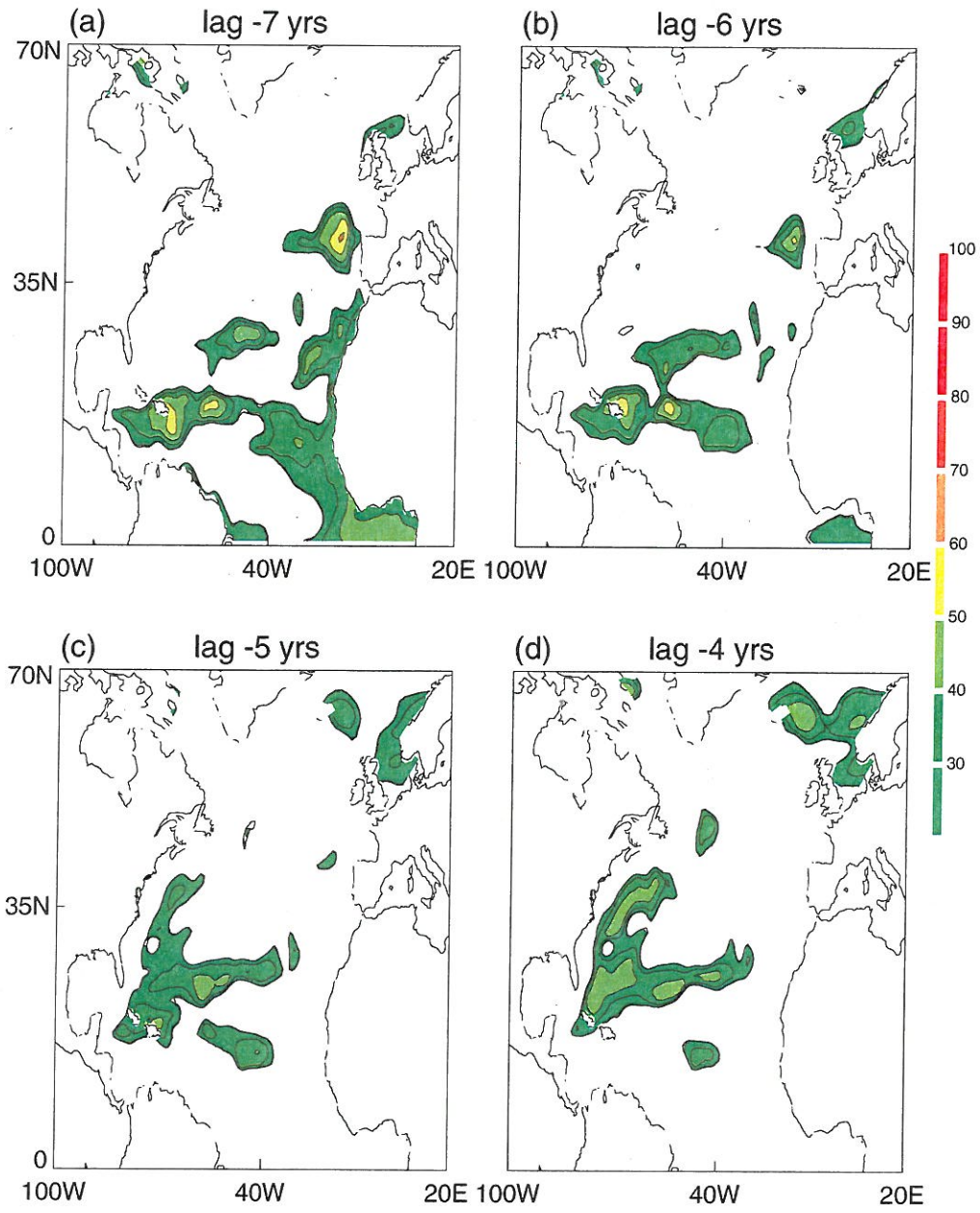


Figure 18: The cross-correlation of the upper 500 $m$ heat content and the time-series of the same dataset averaged over the region shown in Fig. 6 (b). (a) to (d) correspond to the lag of -7 to -4 years, respectively, and, (e) to (h) a lag of -3 to 0 years. The values are cross-correlation coefficient multiplied by 100. Only the absolute values above 30 are contoured to emphasize the decadal variations. Correlations above 0.3 are significant at the 95% level.

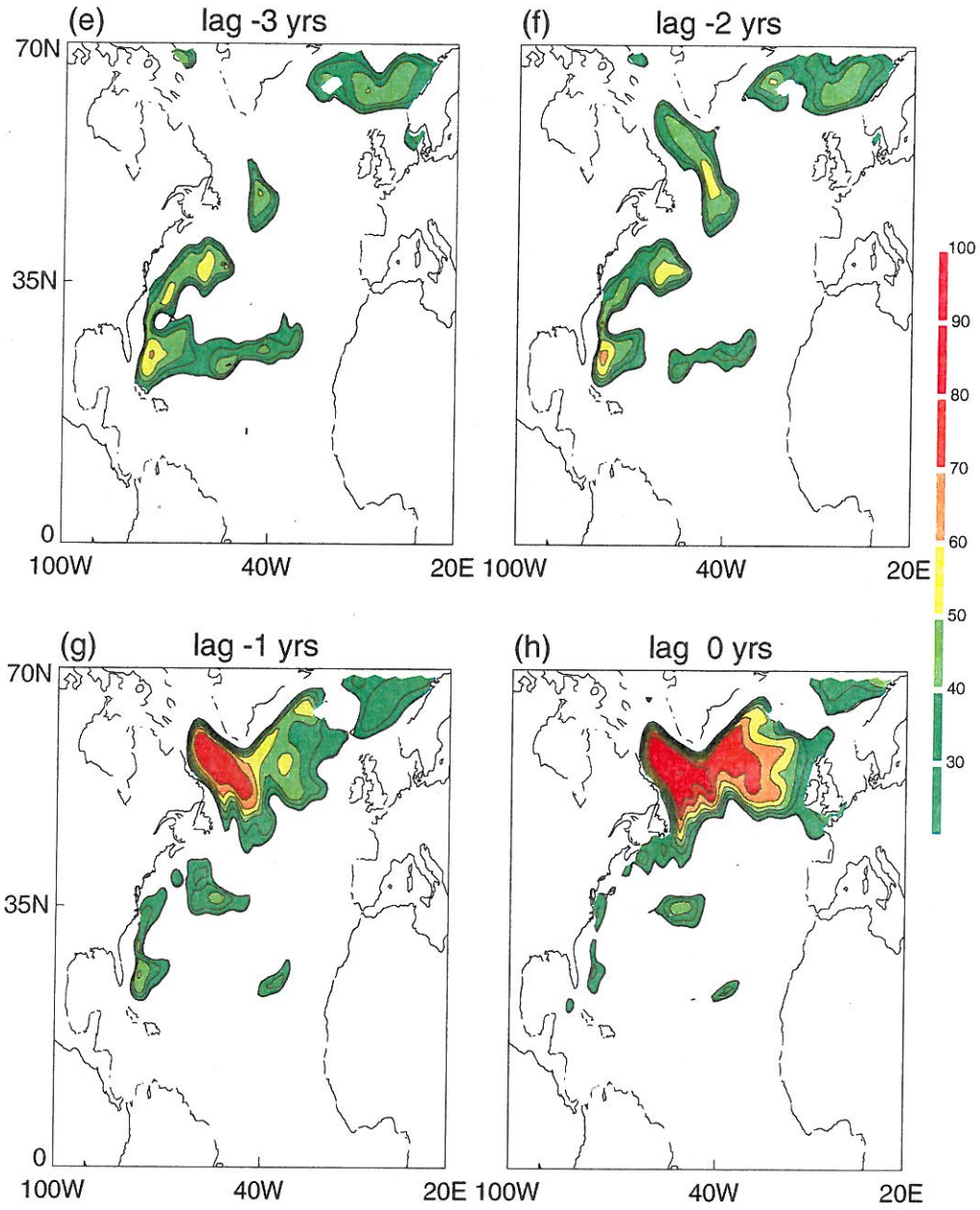


Figure. 18 (cont)

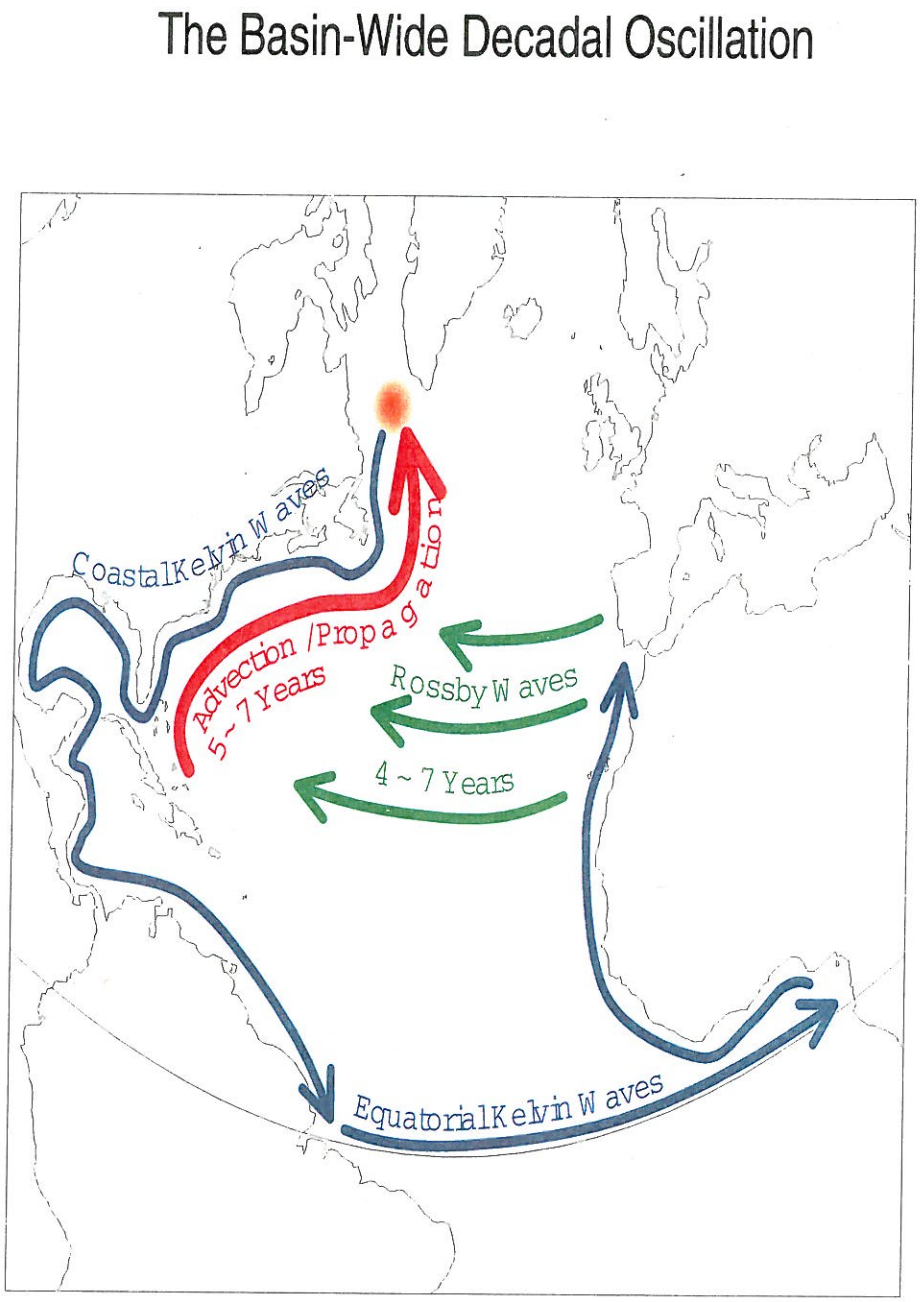


Figure 19: Schematic figure of the mechanism for the basin-wide decadal oscillation

## References


Alverson, K. and W. B. Owens, 1996: Topographic Preconditioning of Open-Ocean Deep Convection. J. Phys. Oceanogr., **26**, 2196–2213.

Barnett, T. P., 1983: Interaction of the Monsoon and Pacific Trade Wind System at Interannual Time Scales. Part I: The Equatorial Zone. Mon. Wea. Rev., **111**, 756–773.

Belkin, I., S. Levitus and J. Antonov, 1996: On the North Atlantic "Great Salinity Anomaly" of the 1980s. Submitted to Prog. Oceanog.

Blumberg, A. F. and G. L. Mellor, 1987: A description of a three-dimensional coastal ocean circulation model, in Three dimensional coastal ocean models. N.S. Heaps, ed., AGU, Washington DC, pp. 1–16.

Curry, R. G. and M. S. McCartney, 1996: Labrador Sea Water Carries North Climate Signal South. Oceanus, **39, 2**, 24–28.

Delworth, T., S. Manabe and R. J. Stouffer, 1993: Interdecadal Variations of the Thermohaline Circulation in a Coupled-Atmosphere Model. J. Clim., **6**, 1993–2011.

Deser, C. and M. L. Blackmon, 1993: Surface Climate Variations over the North Atlantic Ocean during Winter: 1900-1989. J. Clim., **6**, 1743–1353.

Dickson, R. R., J. Lazier, J. Meincke, P. Rhines and J. Swift, 1996: Long-term coordinated changes in the convective activity of the North Atlantic. Prog. Oceanog., **38**, 241–295.

Dickson, R. R., J. Meincke, S.-A. Malmberg and A. J. Lee, 1988: The "Great Salinity Anomaly" in the Northern North Atlantic 1968-1982. Prog. Oceanog., **20**, 103–151.

Frankignoul, C. and K. Hasselmann, 1977: Stochastic climate models, II, Application to sea surface temperature variability and thermocline variability. Tellus, **29**, 284–305.

Gascard, J. C., 1978: Mediterranean deep water formation, baroclinic eddies and ocean eddies. oceanol. Acta., **1**, 313–315.

Gascard, J. C. and R. A. Clarke, 1983: The formation of Labrador Sea water. Part II: Mesoscale and smaller-scale processes. J. Phys. Oceanogr., **13**, 1779–1797.

Greatbatch, R. J., A. F. Fanning, A. D. Goulding and S. Levitus, 1991: A diagnosis of interpendatal circulation changes in the North Atlantic. J. Geophy. Res., **96**, 22009–22023.

Griffies, S. M. and E. Tziperman, 1998: A Linear Thermohaline Oscillator Driven by Stochastic Atmospheric Forcing. J. Clim., **8**, 2440–2453.

Grötzner, A., M. Latif and T. P. Barnett, 1998: A decadal climate cycle in the North Atlantic Ocean as simulated by the ECHO coupled GCM. J. Clim., **11**, 831–847.

Häkkinen, S., 1999: Variability of the simulated meridional heat transport in the North Atlantic for the period 1951-1993. J. Geophy. Res., **104**, No. C5, 10,991–11,007.

Häkkinen, S., 2000: Decadal air-sea interaction in the North Atlantic based on observations and modeling results. J. Clim., **13**, 1195–1219.

Häkkinen, S., 2001: Variability in sea surface height: a qualitative measure for the meridional overturning in the North Atlantic. J. Geophy. Res., submitted.

Häkkinen, S. and G. L. Mellor, 1992: Modeling the seasonal variability of the coupled arctic ice-ocean system. J. Geophy. Res.

Hansen, D. V. and H. F. Bezdek, 1996: On the nature of decadal anomalies in North Atlantic sea surface temperature. J. Geophy. Res., **101, C4**, 8749–8758.

Holland, M. M., C. M. Bitz, M. Eby and A. J. Weaver, 1999: The role of ice-ocean interactions in the variability of the North Atlantic thermohaline circulation. J. Clim., submitted, pp. 1–59.

Holland, W. R. and A. Hirschman, 1972: A numerical calculation of the circulation in the North Atlantic Ocean. J. Phys. Oceanogr., **2(10)**, 336–354.

Horel, J., 1984: Complex principal component analysis: Theory and examples. J. Climate Appl. Meteor., **23**, 1660–1673.

Houghton, R. W., 1996: Surface Quasi-Decadal Fluctuations in the North Atlantic. J. Clim., **9**, 1363–1373.

IPCC, 2000: Summary for policymakers (A Report of Working Group I of the Intergovernmental Panel on Climate Change. pp. 1–20.

Jolliffe, I. T., 1986: Principal Component Analysis. Springer-Verlag, p. 271.

Kara, A. B., P. A. Rochford and H. E. Hurlburt, 2000: An optimal definition for ocean mixed layer depth. J. Geophy. Res., **105, NO. C7**, 16,803–16,821.

Killworth, P. D., 1976: The mixing and spreading phases of MEDOC. I. Progress in Oceanography, **7**, 59–90.

Killworth, P. D., 1983: Deep water convection in the world ocean. Rev. Geophys., **21(1)**, 1–26.

Klinger, B., J. Marshall and U. Send, 1996: Representation of convective plumes by vertical adjustment. J. Geophy. Res., **101 (C8)**, 18,175–18,182.

LabSeaGroup, 1998: The Labrador Sea Deep Convection Experiment. Bull. Amer. Meteor. Soc., **79 (10)**, 2033–2058.

Latif, M. and T. P. Barnett, 1994: Cause of Decadal Climate Variability over the North Pacific and North America. Science, **266, 28 Oct.**, 634–637.

Lilly, J. M., P. B. Rhines, M. Visbeck, R. Davis, J. R. N. Lazier, F. Schott and D. Farmer, 1999: Observing Deep Convection in the Labrador Sea during Winter 1994/95. J. Phys. Oceanogr., **29**, 2065–2098.

Marshall, J. and F. Schott, 1999: Open ocean convection: observations, theory, and models. Reviews of Geophysics, **37,1**, 1–64.

Mauritzen, C. and S. Häkkinen, 1997: Influence of sea ice on the thermohaline circulation in the Arctic-North Atlantic Ocean. Geophy. Res. Lett., **24**, No.24, 3257–3260.

Mellor, G. L. and T. Yamada, 1982: Development of a turbulence closure model for geophysical fluid problems. Rev. Geophys., **20**, 851–875.

Mizoguchi, K., S. D. Meyers, S. Basu and J. J. O'Brien, 1999: Multi- and quasi-decadal variations of sea surface temperature in the North Atlantic. J. Phys. Oceanogr., **29**, No. 12, 3133–3144.

Molinari, R. L., D. A. Mayer, J. F. Festa and H. F. Bezdek, 1997: Multiyear variability in the near-surface temperature structure of the midlatitude western North Atlantic Ocean. J. Geophy. Res., **102, C2**, 3267–3278.

Pickart, R. S., 2000: Is Labrador Sea Water Formed in the Irminger basin? International WOCE Newsletter, **39**, 1–43.

Pickart, R. S., M. A. Spall and J. R. N. Lazier, 1997: Mid-depth ventilation in the western boundary current system of the sub-polar gyre. Deep-Sea Res., **44**, no. 6, 1025–1054.

Reverdin, G., D. Cayan and Y. Kushnir, 1997: Decadal variability of hydrography in the upper northern North Atlantic in 1948-1990. J. Geophy. Res., **102**, 8505–8531.

Reverdin, G. and N. Verbrugge, 1999: Upper ocean variability between Iceland and Newfoundland. J. Geophy. Res., **104, C12**, 29,599–29,611.

Saravanan, R. and J. C. McWilliams, 1998: Advective Ocean-Atmosphere Interaction: An Analytical Stochastic Model with Implications for Decadal Variability. J. Clim., **11**, 165–188.

Sarmiento, J. L. and K. Bryan, 1982: An ocean transport model for the North Atlantic. J. Geophy. Res., **87**, 394–408.

Seager, R., Y. Kushnir, M. Visbeck, N. Naik, J. Miller, G. Krahmann and H. Cullen, 2000: Causes of Atlantic Ocean Climate Variability between 1958 and 1998. J. Clim., **13**, 2845–2862.

Send, U. and J. Marshall, 1995: Integral Effects of Deep Convection. J. Phys. Oceanogr., **25**, 855–872.

Sharp, R. J., 1996: Complex Empirical Orthogonal Function Analysis in Two Dimensional Data Sets: Theory and Examples. Bachelors Thesis at Florida State University.

Shriver, J. F., M. A. Johnson and J. J. O'Brien, 1991: Analysis of Remotely Forced Oceanic Rossby Waves off California. J. Geophy. Res., **96, C1**, 749–757.

Sutton, R. T. and M. R. Allen, 1997: Decadal predictability of North Atlantic sea surface temperature and climate. Nature, **388**, 563–567.

UNESCO, 1981: Tenth report of the joint panel on oceanographic tables and standards. UNESCO Technical Papers in Marine Sci., **No. 36**, UNESCO, Paris.

Visbeck, M., H. Cullen, G. Krahmann and N. Naik, 1998: An ocean model's response to North Atlantic Oscillation-like wind forcing. Geophy. Res. Lett., **25(24)**, 4521–4524.

Visbeck, M., J. Marshall and H. Jones, 1996: Dynamics of Isolated Convective Regions in the Ocean. J. Phys. Oceanogr., **26**, 1721–1734.

Wallace, D. W. R. and J. R. N. Lazier, 1988: Anthropogenic Chlorofluoromethanes in newly formed Labrador Sea Water. Nature, **332**, 61–63.

Weaver, A. J. and E. S. Sarachik, 1991: Evidence for decadal variability in an ocean general circulation model: An advective mechanism. Atmos. Ocean, **29(2)**, 197–231.